Optimisation of single-nuclei isolation and RNA sequencing of parasitic nematodes

Sarah K Buddenborg[1], Alison A Morrison[3], Anna C Fletcher[1], Manuela R Kieninger[1], Bee Ling Ng[1], Kirsty Maitland[2], Emily Hart[4], Dave J Bartley[3], Maria A Duque-Correa[4], Stephen R Doyle[1]

[1]**Wellcome Sanger Institute, Hinxton, Cambridgeshire, CB10 1SA, UK**
Sarah K Buddenborg (sarah.buddenborg@sanger.ac.uk)
Anna C Fletcher (annie.fletcher@sanger.ac.uk)
Manuela R Kieninger (manuela.kieninger@sanger.ac.uk)
Bee Ling Ng (beeling.ng@sanger.ac.uk)
Stephen R Doyle (stephen.doyle@sanger.ac.uk)

[2]**University of Glasgow, SBOHVM, Garscube Campus, G61 1QH**
Kirsty Maitland (kirsty.maitland@glasgow.ac.uk)

[3]**Moredun Research Institute, Pentlands Science Park, Bush Loan, Penicuik, EH26 0PZ, UK**
Alison A Morrison (alison.morrison@moredun.ac.uk)
Dave J Bartley (dave.bartley@moredun.ac.uk)

[4]**Cambridge Stem Cell Institute, University of Cambridge, Cambridge, CB2 0AW, UK**
Emily Hart (ejh200@cam.ac.uk)
Maria A Duque-Correa (mad75@cam.ac.uk)

Abstract

Single-cell/nuclei transcriptomics has revolutionised our understanding of cell, tissue, and organismal biology during health and disease of humans and model organisms. However, for non-model species, reassessment and refinement of conventional methods to address novel technical and biological challenges are needed. Here, we evaluate three established nuclei isolation protocols and, building on experiences, optimised single nuclei isolation for parasitic nematodes (SNIP). We test the versatility of SNIP across diverse species and life stages, validating it with snRNA-seq to reveal sex, stage, and tissue-specific gene expression. Optimised protocols will advance the understanding of parasitic nematodes, from fundamental biology to infection and disease.

Keywords

Single-nuclei RNA-seq, nematodes, helminths, transcriptomics, protocol optimisation

Introduction

With the increasing affordability and availability of high-throughput sequencing and commercial single-cell (sc) and single-nuclei (sn) transcriptomic platforms, cellular-resolution approaches to investigate the biology of non-model organisms are becoming more accessible. Applying sc/snRNA-seq to non-model organisms does, however, bring new biological and technical challenges that may need to be overcome. For example, the biological richness of non-model organism diversity brings a diversity of cell and tissue types that vary in their morphology and composition and will differ in their sensitivities toward cellular and nuclei dissociation. Further, sample access may be impacted by geographic or biological constraints, limiting the availability of or access to fresh material. Understanding and overcoming these challenges will likely require organism-specific biological knowledge. Therefore, conventional, well-established methods developed for model organisms may need adaptation and refinement for use in non-model organisms.

A field with exclusively non-model organisms that stands to benefit greatly from understanding biology at a single-cell resolution is parasitology. scRNA-seq of single-cell eukaryotic parasites such as *Plasmodium spp.* and *Trypanosoma spp.* has been particularly

successful, with significant advances made in understanding life stage-specific gene expression patterns and transitions during their life cycles, mechanisms of infection and disease progression, as well as identifying new drug targets for interrupting transmission [1–7]. In contrast, the application of scRNA-seq for multicellular parasites has encountered distinct challenges due to vast differences in life history traits and hosts and great diversity in body plan and cellular composition between and even within species throughout their life cycles. Multicellular parasites are exposed to variable environmental conditions inside and outside the host, necessitating a toughened outer coating (i.e. cuticle, tegument, exoskeleton), which presents a major obstacle for single-cell/nuclei isolation. Further, because most species cannot be cultured *in vitro*, access to obligate parasitic stages can be geographically restricted and difficult or impossible to collect without sampling post-mortem. Despite these challenges, there are a growing number of single-cell life-stage atlases for parasitic helminths including the trematodes *Schistosoma mansoni* [8–11] and *Fasciola hepatica* [12]. More recently, cell atlases have been generated for *Brugia malayi* microfilariae [13], *Ascaris suum* intestinal tissue [14], *Haemonchus contortus* embryos [15], and *Heligmosomoides bakeri* mixed-sex adults [16]. These studies often exploit protocols developed for mammalian tissues, although it is unclear how transferable and efficient these different single-cell isolation methods are for diverse species and life cycle stages of parasitic helminths.

In this study, we have tested and compared three widely-used single nuclei isolation protocols for use in snRNA-seq of parasitic nematodes. We focused on isolating single nuclei as opposed to single cells because frozen material can be used, providing many advantages, including sampling across life stages, the ability to collect and store samples over time, and simultaneous processing to minimise batch effects. Building on our experiences from the three-protocol comparison, we have developed a new nuclei isolation protocol and tested it on multiple life cycle stages and sexes of two gastrointestinal parasitic nematodes, *Haemonchus contortus* and *Trichuris muris*. We assessed the nuclei preparations from our protocol using the Parse Biosciences Evercode WT platform for snRNA-seq and Illumina sequencing. Here, we provide the protocol and discuss some of the challenges and opportunities of sc/snRNA-seq approaches to advance the adoption of this technology in non-model organisms and its applications to better understand helminth biology.

Results

Comparison of three existing nuclei isolation protocols

To optimise a protocol for generating single nuclei suspensions from parasitic nematodes, we first compared the strengths and limitations of three established isolation protocols: (i) a *Caenorhabditis elegans* nuclei isolation protocol (hereinafter referred to as “Celegans”) [17,18], (ii) a Human Cell Atlas (HCA) protocol [19], and (iii) the Frankenstein protocol [20]. The Celegans protocol was the only protocol explicitly used for a nematode. The HCA protocol has been extensively used on a wide range of mammalian tissues as part of the Human Cell Atlas Project [21]. The Frankenstein protocol [20] was chosen for its positive reputation amongst the 10X Genomics user community. An overview of the four key steps of the three protocols is shown in **Figure 1 A**, which include tissue disruption, cell lysis and dissociation, homogenisation, and debris removal. Each protocol was performed using ten frozen adult female *H. contortus* worms to enable comparison between protocols.

Tissue disruption

Tissue disruption is the first stage of the process and involves breaking the tissue to reveal the cellular contents within. This step is particularly important for nematodes, which have a highly cross-linked acellular cuticle that, depending on the organism's life history or life stage, provides protection from its environment, either inside or outside a host.

The HCA and Frankenstein methods involve mincing the tissue into smaller pieces using a scalpel, while the Celegans method does not include a tissue disruption step; however, considering *C. elegans* small size (~1 mm x 50 µm), exposure of cellular contents occurs during homogenisation below.

Cell Lysis

The lysis step breaks down tissue and disrupt cellular membranes to make the nuclei accessible. The lysis buffer works in conjunction with mechanical homogenisation to create a nuclei suspension. Thus, the effectiveness of the lysis buffer, on its own, is not easily measured.

Different lysis buffers are used in each protocol, although all lysis buffer recipes typically contain the same four basic ingredients: 1) detergent to disrupt the cell membrane (e.g. Triton X-100, SDS); 2) pH stabiliser (e.g. HEPES, Tris-HCl); 3) salt to add ionic strength to facilitate cell disruption (e.g. $MgCl_2$ $NaCl_2$, KCl); and 4) RNase inhibitor to protect RNA degradation (e.g. DTT, recombinant enzyme RNase inhibitor, EDTA). Additional RNase inhibitor was not added to the commercial lysis buffer used in the Frankenstein protocol.

Homogenisation

Homogenisation aims to completely release the cells from tissues and nuclei from cells, ensuring the suspension is free from clumps. The Celegans and HCA protocols use a glass Dounce tissue grinder to achieve a single nuclei suspension. The Celegans protocol uses ten strokes with the tight Dounce tissue grinder pestle followed by two sets of ten strokes with a plastic micro-pestle. In between each homogenisation set, the nuclei suspension is collected using low-speed centrifugation to separate it from large undigested tissue and avoid over-homogenisation. The HCA homogenisation step required continuous homogenisation with the Dounce tissue grinder with 10-20 strokes. In contrast, the Frankenstein protocol only used a plastic micro-pestle, a 5-minute incubation in the lysis buffer, and mixing with a wide-bore pipette tip.

We examined the samples after the homogenisation stage by microscopy to determine the amount of intact tissue vs empty cuticles **(Figure 1 B)**. Empty cuticle debris was observed in the Celegans protocol, showing complete tissue homogenisation with the tight Dounce tissue grinder pestle. Large fragments of worms were prominent in the HCA and Frankenstein homogenates, indicating incomplete homogenisation.

Debris removal

The preceding steps generate significant amounts of debris, including acellular material that cannot be digested or homogenised and cellular material resulting from cell lysis. Large debris (>30 µm) can cause clogs or wetting failures in microfluidics-based library protocols [22], such as 10X Genomics, but presents less of a problem in combinatorial indexing strategies in which nuclei are distributed in microtitre plates. Nonetheless, small debris (<30 µm) may contain ambient RNA, increasing the transcriptional background noise [23], and should be removed.

All three protocols used at least one strainer for large debris removal and one wash for small debris removal. The Celegans protocol utilises low-speed centrifugation, buffer wash, and a 40 µm strainer. The HCA protocol strains the homogenate through a 40 µm filter, followed by a wash and Percoll density gradient. In the Frankenstein method, the homogenate is cleaned through a 70 µm strainer, washed, and then passed through a 35 µm strainer. Large debris was easily removed in all three protocols with cell strainers. Small debris was observed in all three protocols but was most visually abundant in the Celegans protocol **(Figure 1 B)**. The Percoll density gradient used in the HCA protocol did not remove more small debris than the other protocols but doubled the protocol time **(Figure 1 B)**.

Outcome

The resulting nuclei suspensions of the three protocols were assessed based on the total nuclei, RNA concentration, and nuclei morphology. Using ten female *H. contortus* worms as input, the Celegans, HCA, and Frankenstein protocols resulted in a mean recovery of 7,700 ± 1,540 standard deviation (SD), 19,227 ± 3,520 SD, and 13,678 ± 1,265 SD nuclei, respectively **(Figure 1 C)**. Comparison of the three protocols revealed a significant difference between Celegans and HCA (p = 0.0065; t(4) = 5.1960), and Celegans and Frankenstein (p = 0.0065; t(4) = 5.1951), but was not statistically significant between HCA and Frankenstein (p = 0.0620; t(4) = 2.5690). Analysis of RNA concentration revealed that the Frankenstein protocol recovered the highest amount of RNA (11,790pg) followed by the HCA and Celegans protocols (7,770 pg and 5,940 pg), respectively. The RNA concentrations were below the assay limits for reporting an RNA integrity number (RIN); however, consistent with concentration, the Frankenstein protocol presented the most prominent 18S and 28S ribosomal RNA peaks on the High Sensitivity RNA tapestation gel (**Figure 1 D**). Considering the nuclei count from the replicate used for RNA extraction from the Celegans, HCA, and Frankenstein protocols, we isolated 0.52 pg of RNA/nucleus, 0.41 pg of RNA/nucleus, and 0.81 pg of RNA/nucleus, respectively. Finally, we assessed nuclei morphology to compare suspensions from the three protocols (**Figure 1 E**). We observed notable degradation of the nuclear envelope in the Celegans protocol nuclei, which, in part, explains the poorer RNA recovery. An example of this can be seen in the FITC-SYBR Green I and overlay images of the nucleus isolated using the Celegans protocol in **Figure 1 E;** a broken nuclear membrane is shown leaking fluorescently stained nucleic acid contents. In contrast, most nuclei isolated from the Frankenstein protocol have smooth and intact membranes, and various nuclei sizes were recovered, suggesting the recovery of nuclei from diverse cell types.

In summary, the Frankenstein protocol generated the most RNA per nucleus and the most consistent morphologically robust and diverse nuclei despite slightly lower total nuclei recovered than the HCA protocol.

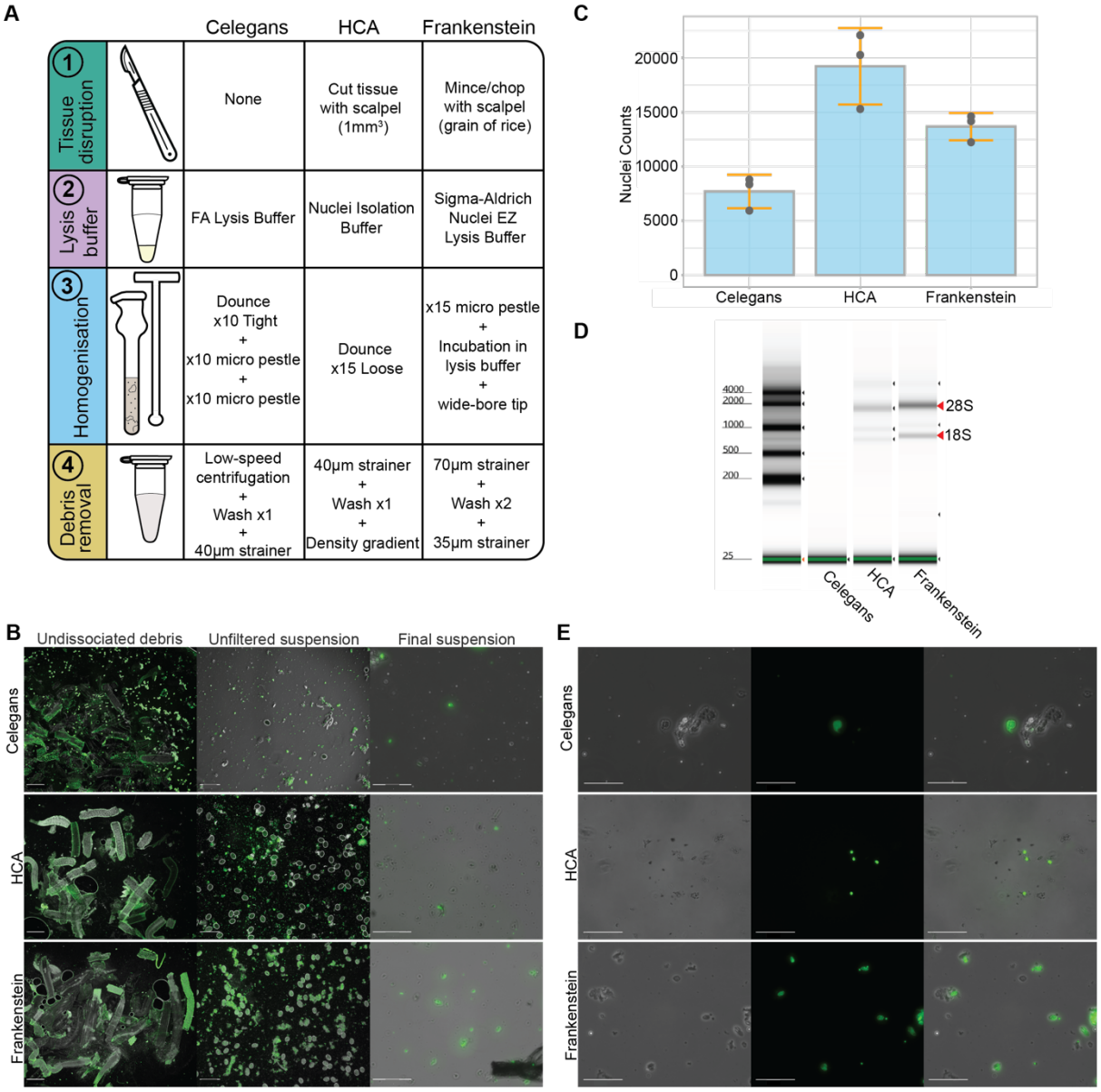

Figure 1. Nuclei isolation of adult female *Haemonchus contortus* worms using three representative protocols. A) Schematic comparison of the three nuclei isolation methods; B) Representative images from the Celegans, HCA, and Frankenstein protocols of the undissociated debris remaining after homogenisation, unfiltered suspension, and final washed nuclei suspensions. Images are overlays of phase contrast and fluorescent microscopy of SYBR Green I-stained samples. Scale bars = 500, 250, and 50 µm for "Undissociated debris", "Unfiltered suspension", and "Final suspension", respectively. C) Manual nuclei counts from each protocol. Error bars represent the standard deviation of the mean of three replicates; D) Representative Agilent HS RNA Tapestation gel of RNA extracted from nuclei suspensions from each protocol; E) Representative phase contrast and SYBR Green I stained fluorescent images of the final nuclei suspensions. Scale bars = 50 µm.

205 ## Optimisation of the **S**ingle **N**uclei Isolation of **P**arasites (**SNIP**) protocol

206 Next, we sought to improve nuclei isolation in parasitic nematodes based on lessons learned
207 from performing the three initial protocols. The key stages of the optimised protocol are
208 outlined in **Figure 2 A** and summarised in **Table 1**.
209
210 We used frozen worms, which enabled greater flexibility in collecting and storing samples
211 before processing. However, one disadvantage of the HCA and Frankenstein protocols was
212 that the tissue was minced or chopped with a scalpel in a petri dish on wet ice, resulting in
213 the worms immediately thawing, which could lead to degraded RNA and decreased nuclei
214 quality if not processed quickly. To prevent this, for the macroscopic stages (e.g. adult
215 worms of *H. contortus* and *T. muris*) we used spring scissors to cut through the cuticle and
216 obtain <2 mm pieces in the sample tube on dry ice. We ground the microscopic stages (e.g.
217 larvae of *H. contortus*) using a mortar and pestle placed in dry ice. This technique enabled
218 the tissue to be kept in a single tube and minimised sample loss, which is important when
219 the starting material is limited, while keeping the sample frozen.
220
221 Damaged nuclei release soluble, “sticky” DNA, which can result in the clumping of intact
222 nuclei. To address this, we included a DNase I enzyme and required $MgCl_2$ in the lysis
223 buffer. Similarly, when lysing cells for single nuclei isolation, RNases are released; thus, to
224 prevent RNA degradation, we added an RNase inhibitor to both the lysis and wash buffers.
225 We note that several RNase inhibitors are commercially available; however, some brands
226 have been associated with lower cDNA yield when used for particular scRNA-seq protocols
227 and technologies [24]. Therefore, we suggest selecting a recommended RNase inhibitor
228 based on the intended downstream single-cell platform.
229
230 The Frankenstein and HCA protocols resulted in a large amount of undigested tissue,
231 whereas homogenisation in the Celegans protocol was too harsh (**Figure 1 B**). Therefore,
232 we optimised the Dounce homogenisation, focusing on the number of strokes and using
233 different-sized Dounce tissue grinder pestles. We found that five strokes with the loose
234 Dounce tissue grinder pestle exposed worm tissue that had not been adequately disrupted
235 with scissors in the previous step and released the first nuclei from well-exposed tissue
236 pieces. Then, using the tight Dounce tissue grinder pestle, tissue and cells were lysed to
237 release the maximum number of nuclei. After each set of strokes with the Dounce tissue
238 grinder pestles, the large undigested tissue pieces were allowed to settle for up to 4 minutes,
239 and the suspended nuclei in the supernatant were collected to prevent lysis from further
240 homogenisation. This additional short incubation in the lysis buffer allowed the complete

241 lysis of the cells within larger chunks of worm tissue. Collecting the nuclei suspension
242 throughout the homogenisation is a step taken from the Celegans protocol. Homogenisation
243 was deemed complete when the suspension was clear to the naked eye.
244
245 Removing both small and large debris in nematode nuclei suspensions is necessary due to
246 the amount of debris generated from the cuticle and lysed cells; however, each method and
247 iteration of debris removal results in nuclei loss and additional processing time. We found
248 large debris was best removed by allowing the debris to settle by gravity during dissociation
249 and filtering the final suspension through a 30 µm cell strainer. To ensure maximal recovery
250 and minimise nuclei loss, we washed the cell strainer with additional wash buffer and
251 pipetted the suspension through on the side of the filter with the tip against the mesh.
252 However, we found the only effective and efficient way to remove small debris from the
253 nuclei suspensions was through Fluorescence-Activated Cell Sorting (FACS). Small cellular
254 and cuticle debris, abundant in the pre-sorted female *H. contortus* sample (**Figure 2 B**), are
255 removed efficiently with FACS (**Figure 2 C**). The gating strategy for selecting SYBR Green I
256 positively stained nuclei for FACS was determined using an unstained negative control
257 (**Supplementary Figure 1)**.
258
259 We compared the nuclei count and RNA quality of our optimised nuclei isolation protocol
260 with those of the three tested protocols. When starting with the same amount of adult worms,
261 the optimised protocol had a mean recovery of 31,797 nuclei which is 4.1-fold more nuclei
262 than the Celegans protocol (p = 0.0001, t(4) = 18.8851), 1.7-fold more than the HCA protocol
263 (p = 0.0049, t(4) = 5.6394), and 2.3-fold more nuclei than the Frankenstein protocol (p =
264 0.0001, t(4) = 15.4725). RNA concentration for the optimised protocol was 210.0 ng, which
265 equated to approximately 2.62 pg/nucleus; this equated to a 3.23-fold increase in RNA
266 received per nucleus relative to 0.81 pg/nucleus from the previous best-performing
267 Frankenstein protocol. The resulting nuclei have smooth nuclear membranes, and very few
268 nuclei showed signs of damage (**Figure 2 B, C**), indicating a high-quality suspension to
269 proceed with sequencing library preparation.

270 **Table 1. Critical steps in protocol optimisation**

Protocol step	Modification	Description
Tissue disruption	Cut frozen worms in the sample tube on dry ice using spring scissors	Cutting worms with scissors on dry ice exposes internal tissues for lysis and reduces RNA degradation, loss of sample and balanced homogenisation
Lysis	Sigma-Aldrich Nuclei EZ Lysis Buffer, with the addition of 0.2 U/µL RNase Inhibitor, 25 µg DNase I, 5 mM $MgCl_2$	DNase I digests any "sticky" free DNA from nuclei that lyse, preventing clumping; $MgCl_2$ is required for DNase I activity and stabilises chromatin; RNase Inhibitor protects RNA in nuclei from degradation by RNases released during tissue/cell lysis
Homogenisation	1 mL Wheaton Dounce tissue grinder 5x loose pestle, 3x tight pestle (repeat 3x tight pestle up to 3x)	Glass Dounce tissue grinder resulted in better homogenisation of the worms than plastic pestles
	Each douncing set is followed by a 2 min incubation on ice to allow large undissociated worm fragments to settle, and nuclei in suspension are collected	Collecting nuclei after each Dounce homogenisation set eliminates the risk of over-douncing and lysing nuclei. Incubating the suspension on ice after each Dounce homogenisation set maximises the effectiveness of the lysis buffer.
Debris removal	1x wash using 2% BSA-PBS with 0.2 U/µL RNase Inhibitor and 5 mM EDTA	Only one wash, using a higher percentage of BSA with RNase Inhibitor added, is performed to minimise the loss of nuclei. Pre-filtering the homogenate through a 70 µm strainer is not necessary when collecting the homogenate after each Dounce homogenisation set because the large debris remains settled in the bottom of the Dounce tube.
	30 µm CellTrics filter, then FACS	A 30 µm strainer removes nematode eggs; washing the CellTrics filter after filtering the homogenate increases the recovery of nuclei
Miscellaneous	Low-binding pipette tips and tubes	Low-binding tips can increase recovery; they can be BSA-blocked for increased recovery
	5 mL Eppendorf Protein LoBind tubes	Increased recovery is observed with LoBind tubes that can fit in a 15 mL adapter in a swing-bucket rotor; they can be BSA-blocked for increased recovery
	Swing-bucket benchtop centrifuge	Swing-bucket rotor pellets nuclei at the bottom of the tubes and results in a lower likelihood of disturbing the pellet during washes

271

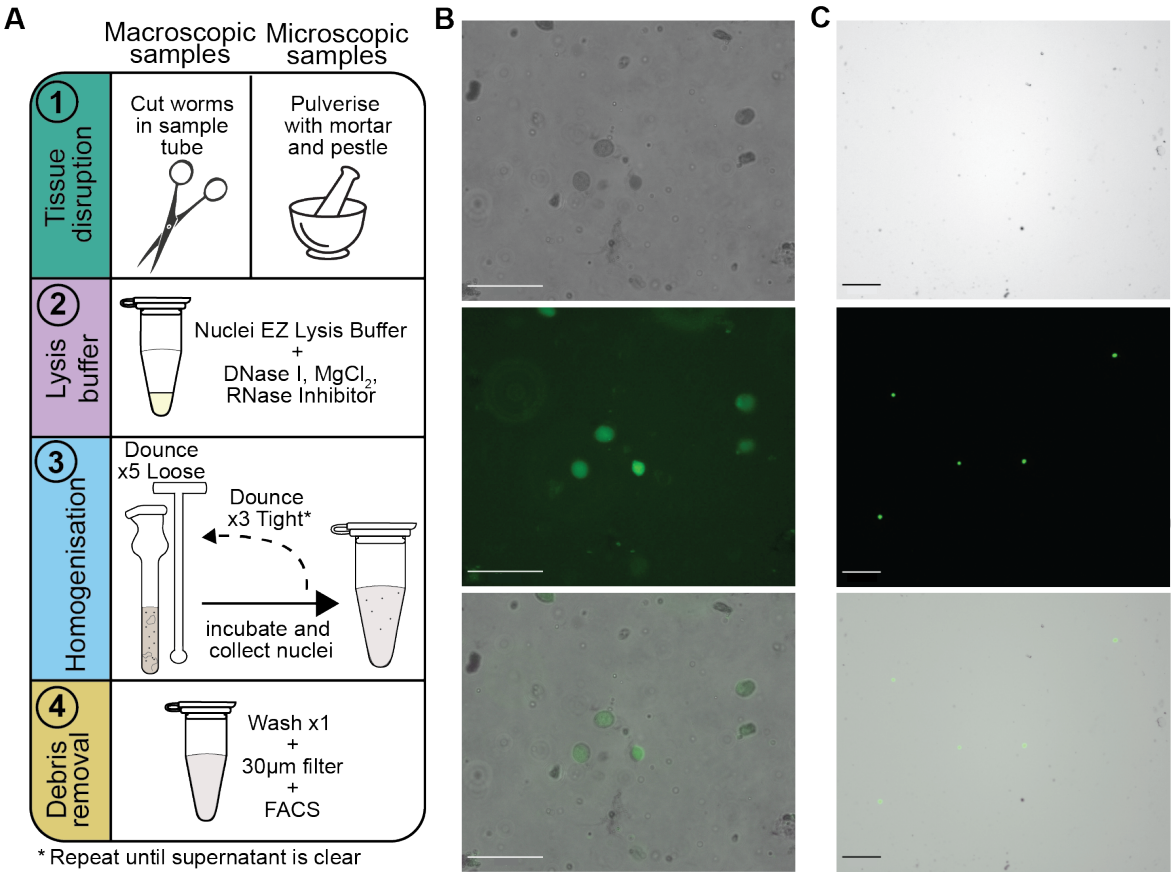

Figure 2. Overview of the Single **N**uclei Isolation of **P**arasites (**SNIP**) **protocol.** A) Schematic comparison of the optimised SNIP protocol for macroscopic (adult worms) and microscopic (eggs and larvae) samples; B) Representative phase contrast, SYBR Green I stained fluorescent, and overlay images of nuclei after washing and filtering. Scale bar = 50 µm; C) Representative images of the *H. contortus* adult female nuclei suspension after debris removal by FACS. Scale bar = 100 µm.

Validation of the SNIP protocol on multiple life stages of *H. contortus and T. muris*

Once optimised, we further tested our protocol with adult male, adult female, and third-stage (L3) larvae of *H. contortus* and with adult female and male *T. muris* (mouse whipworm), a biologically and phylogenetically distinct parasitic nematode species [25].

The microscopic size of L3 larvae of *H. contortus* precludes the use of scissors to cut the cuticle of the worms in the tissue disruption step of our protocol. Therefore, to ensure tissue

290 disruption of this life stage, we ground the frozen larval pellet using a porcelain mortar and
291 pestle on dry ice and then transferred the sample to the Dounce tube using a microspatula.
292 Next, we optimised the number of sets of Dounce homogenisation strokes with the tight
293 Dounce tissue grinder pestle. Homogenisation of the macroscopic adult worm samples was
294 completed after one set of the loose Dounce tissue grinder strokes and two sets of tight
295 Dounce tissue grinder strokes, as evidenced by a clear supernatant in the Dounce tube. In
296 contrast, L3 larvae did not homogenise as easily and required additional sets of
297 homogenisation with the tight Dounce tissue grinder pestle until the supernatant in the
298 Dounce tube was clear to the naked eye. This was validated by fluorescent staining of
299 aliquots of the supernatant after each round. In our hands, a maximum tissue volume
300 equivalent to 20 µL per 1 mL Dounce capacity was optimal without requiring excessive time
301 to complete homogenisation. Importantly, additional sets of the tight Dounce tissue grinder
302 strokes do not result in nuclei lysis because the supernatant containing nuclei is collected
303 after each Dounce homogenisation set.
304
305 Manual nuclei counts for three independent replicates of each species and life stage tested
306 are shown in **Figure 3 A**. Although our protocol was optimised using female *H. contortus,* it
307 proved even more effective on the female *T. muris* samples; the number of nuclei isolated
308 per worm was significantly higher in the adult female *T. muris* ($\bar{x}$ = 26,675.33 nuclei/worm)
309 than in *H. contortus* ($\bar{x}$ = 3,570 nuclei/worm) (p = 0.0001, t(4) = 15.9198). This is, in part,
310 explained by the differences in parasite size; adult female *H. contortus* worms are between
311 20-30 mm x 300-500 µm, and adult female *T. muris* worms are 35-50 mm x 40-600 µm. The
312 large range in width of *T. muris* is due to its whip-like intracellular anterior end. RNA recovery
313 was 210.0 ng for *H. contortus* females, 37.9 pg for *H. contortus* males, 23.9 ng for *H.*
314 *contortus* L3s, 901.6 ng for *T. muris* females, and 2,310.0 ng for *T. muris* males. This
315 equates to approximately 2.62 pg/nucleus for *H. contortus* females, 0.53 pg/nucleus for *H.*
316 *contortus* males, 0.17 pg/nucleus for *H. contortus* L3s, 1.66 pg/nucleus for *T. muris* females,
317 and 2.50 pg/nucleus for *T. muris* males.
318
319 The FACS analysis of samples collected and fixed for snRNA-seq is shown in **Figure 3 B**.
320 Nuclei were sorted on a SYBR Green I positive signal (shown in the green box) with
321 percentages of total events presented (**Figure 3 B**). An aliquot of unstained nuclei was used
322 to determine gating for a SYBR Green I positive signal (FACS plots shown in
323 **Supplementary Figures 1-2**). The distinct clusters of SYBR Green I fluorescence-positive
324 nuclei in the adult worm samples reflect different levels of ploidy within nuclei populations
325 that, while well understood in the free-living model nematode *C. elegans* [26], are observed
326 here for the first time for *H.contortus* and *T. muris.*

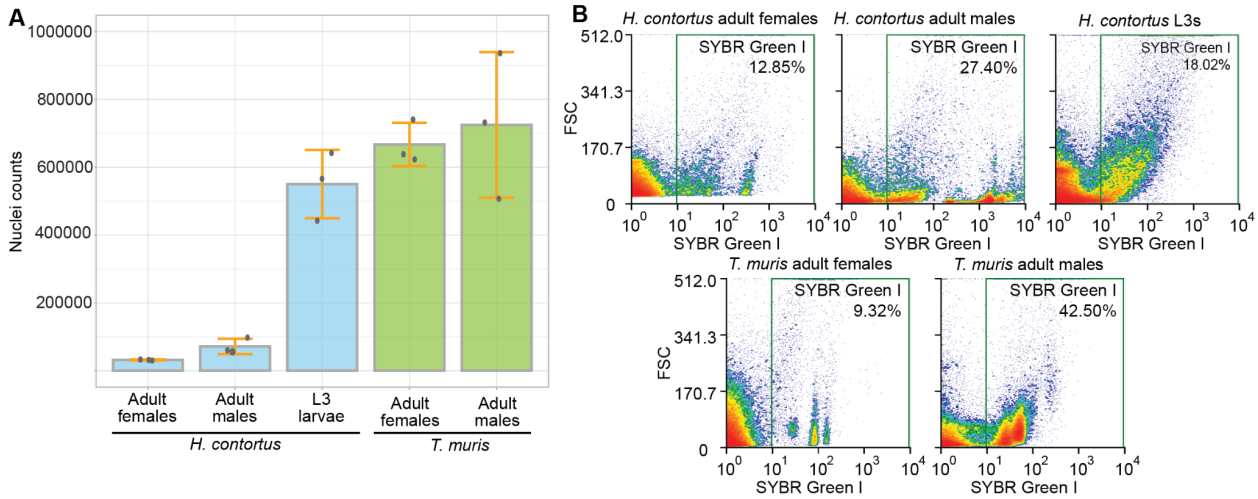

Figure 3. Comparison of the Single **N**uclei Isolation of **P**arasites (**SNIP**) **protocol on different species and life stages.** A) Nuclei counts of each species and stage using the SNIP protocol. For *H. contortus*, ten adult females, 20 adult males, and ~250,000 microscopic L3 larvae were used per replicate (n = 3), which was approximately the same volume per tube. For *T. muris*, 25 adult female and 25 male parasites were included per replicate (n = 3). B) Representative Fluorescence-Activated Cell Sorting (FACS) plots of each species and stage tested using the optimised nuclei isolation protocol. Gating for a positive SYBR Green I signal was determined based on an unstained negative control nuclei aliquot from each sample (shown in **Supplementary Figure 2**). The x-axis displays SYBR Green I fluorescence in log scale using the 488 nm laser and 507/19 filter. The y-axis is the forward scatter area (FSC-A) on a linear scale.

Single nuclei RNA sequencing identifies distinct cellular populations in different parasite life stages

To validate our optimised nuclei isolation protocol, we performed snRNA-seq on the nuclei suspensions obtained from the different species and life stages. We chose to use the Parse Biosciences Evercode platform, based on Split Pool Ligation-based Transcriptome sequencing (SPLiT-seq) [27], over other commercial high-throughput platforms, such as 10X Genomics Chromium, primarily to enable greater flexibility in sampling different life stages throughout a life cycle (in preparation for developmental cell atlases). Specifically, with this technology, nuclei preparations from individual stages could be collected at different times, fixed, and stored frozen for up to six months before library preparation, enabling the processing of different samples together and thus minimising a source of technical bias between samples and replicates.

353
354 We performed two rounds of library preparation and sequencing, designated “experiment 1”
355 and “experiment 2,” using the Parse Biosciences Evercode WT Mini kit. This kit allows up to
356 10,000 nuclei to be sequenced per experiment and distributed between 1 and 12 samples.
357 **Table 2** shows the total nuclei and median genes and transcripts per nucleus from
358 sequencing nuclei libraries of the two parasites and different life stages from experiments 1
359 and 2. The number of wells per sample was determined for both experiments based on the
360 starting nuclei concentration. In experiment 1, we obtained consistent counts of genes and
361 transcripts per nuclei for all stages. However, the total nuclei counts were more variable, with
362 higher counts for *T. muris* adult females (n = 1,317) and lowest for *H. contortus* adult males
363 (n = 224). For experiment 2, we increased the number of starting nuclei, which increased the
364 number of total nuclei recovered. However, this experiment was also variable and was
365 somewhat dependent on the starting nuclei concentration; here, the nuclei counts of *T. muris*
366 adult males were lower concentration and required three wells, whereas the counts for *H.*
367 *contortus* L3 were higher and only required one well.
368
369 The sequencing aimed to validate the library preparation approach on various sample inputs,
370 not to generate comprehensive scRNA-seq data for a full description of transcriptional
371 variation, which requires far larger numbers of nuclei or cells per sample. Nonetheless,
372 despite low sample input, analysis of transcript expression per species revealed clusters of
373 nuclei based on: 1) life stage and sex (**Figure 4 A,F** for *H. contortus* and *T. muris*,
374 respectively); and 2) clustering of nuclei that were shared or unique to life stages and cell
375 and tissue-specific variation and differentiation (**Figure 4 B,G**). Here, we have inferred the
376 putative function of each cluster based on gene set enrichment and orthology from the
377 model free-living nematode *C. elegans*, revealing stage and tissue-specific gene expression
378 such as putative mechanosensory neurons in *H. contortus* L3 (**Figure 4 C**) and vulval
379 muscle (**Figure 4 D**) and sensory neurons (**Figure 4 E**) specific to adult female and males,
380 respectively. Similar stage and tissue-specific expression were observed in *T. muris*,
381 highlighting nuclei associated with gametogenesis (**Figure 4 H**) and highly distinct neurons
382 (**Figure 4 I**) specific to males, as well as a cluster highly enriched in WAP-domain/S1
383 peptidase protein expression-specific to females (**Figure 4 J**). We acknowledge that
384 significant evolutionary and phylogenetic differences between *C. elegans* and the parasite
385 species examined here mean that “marker genes” used to characterise a cell or tissue type
386 must be applied cautiously. Considering the sparse functional annotation information for
387 non-model species such as parasitic nematodes [28], data such as these represent both a
388 challenge and an opportunity for improving genomic resources for these species and toward
389 building more comprehensive cell and nuclei atlases for understanding their biology.

390

391

392 **Table 2: Comparison of nuclei sequencing of different species and life stages from**

393 **two experiments**

		Experiment 1				Experiment 2			
Species	**Stage**	**Wells[1]**	**Nuclei**	**Genes/ nucleus[2]**	**Transcripts/ nucleus[2]**	**Wells**	**Nuclei**	**Genes/nucleus**	**Transcripts/ nucleus**
Haemonchus contortus	**Adult male**	2	224	288	496	2	412	1,277	3,740
	Adult female	2	553	332	521	2	3,867	833	2,043
	L3	2	645	333	476	1	2,159	477	646
Trichuris muris	**Adult male**	2	609	356	604	3	55	243	366
	Adult female	2	1,317	260	512	2	1,129	54	84

394

395 1. Wells: the number of wells of the 12-well Parse mini kit used per life stage.

396 2. The number of genes and transcripts per nucleus reflect median values.

397

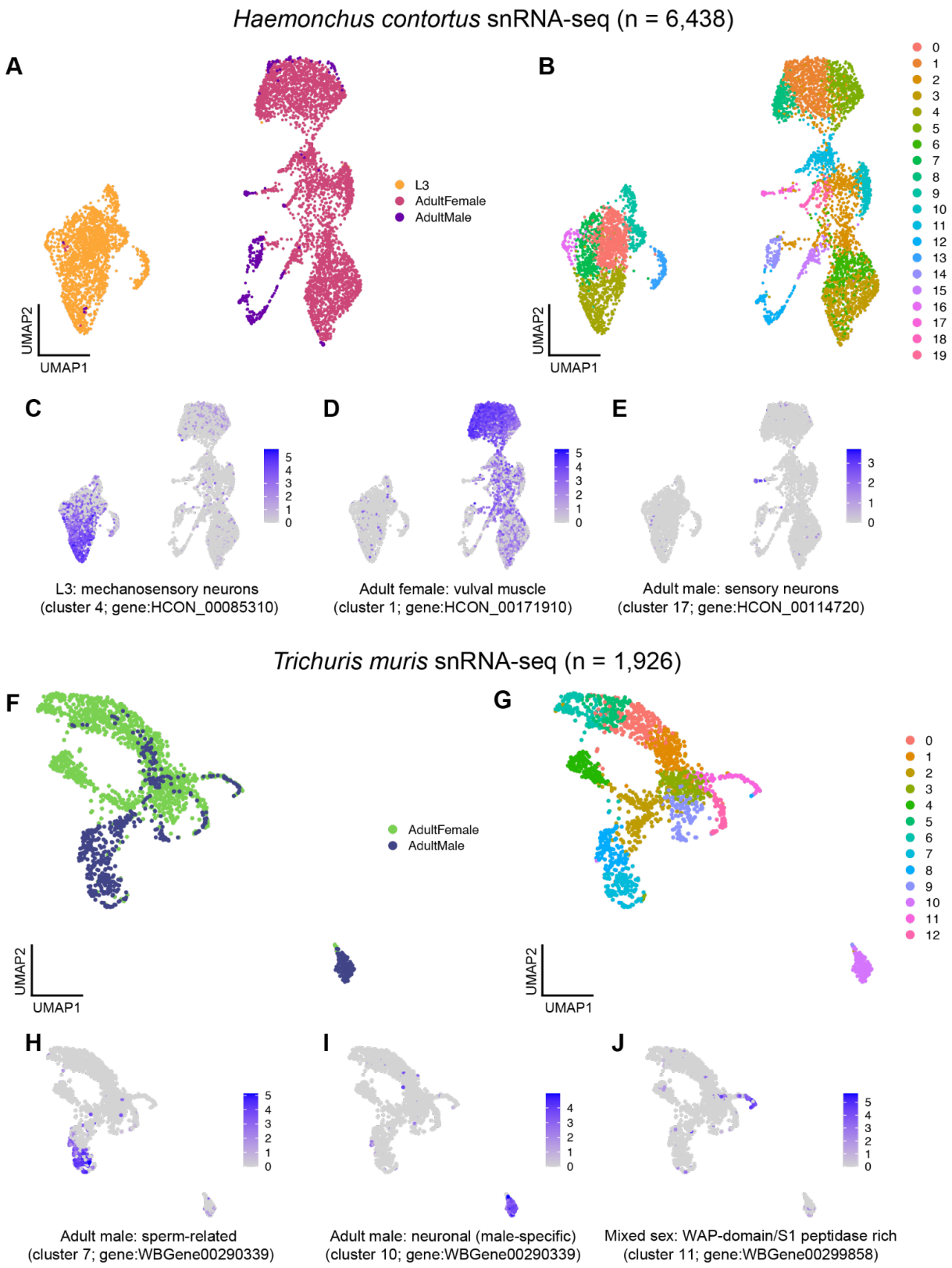

Figure 4: Single-nuclei RNA sequencing of different life stages of *Haemonchus contortus* and *Trichuris muris.* Uniform Manifold Approximation and Projections (UMAPs) of snRNA-seq data from (A-E) *H. contortus* (n = 6,438 nuclei from experiment 2) and (F-J) *T.*

403 *muris* (n = 1,926 nuclei from experiment 1) coloured by (A, F) life stage or nuclei cluster (B,
404 G). In total, 20 nuclei clusters were predicted from three life stages (adult male, adult female,
405 L3) of *H. contortus*, and 13 nuclei clusters from two life stages (adult male, adult female) of
406 *T. muris*. In C-E and H-J, we highlight three examples of biologically meaningful clusters
407 from both datasets, demonstrating sex and stage-specific gene expression (colour scale: log
408 normalised expression counts) with inferred functional roles based on *Caenorhabditis*
409 *elegans* orthology and gene set enrichment from the top 20 differentially expressed genes
410 per cluster. Clustering was performed using Seurat in R.

411

412 # Discussion

413 In this study, we evaluated three existing protocols for isolating single nuclei for snRNA-seq,
414 from which we optimised a method for recovering nuclei from parasitic nematodes (SNIP).
415 Our motivation for this work is to create robust cell atlases to better understand parasitic
416 nematode development, shed light on the tissues and organs that mediate interactions with
417 their hosts, and discover novel drug targets and mechanisms of drug resistance. Here, we
418 discuss the rationale of our approach, challenges faced, and ongoing limitations to be
419 overcome towards applying snRNA-seq for parasitic nematodes specifically, but more
420 generally, the application of cellular-resolution technologies toward other complex and
421 enigmatic non-model organisms.
422
423 The use of single-cell and single-nuclei RNA sequencing to understand the fundamental
424 biology of organisms at cellular resolution is advancing rapidly. Although there are
425 successful examples of cell atlases of specific life stages or tissues of multicellular parasites
426 using scRNA-seq [8–14,16], we specifically chose to use snRNA-seq for several reasons.
427 First, we want to collect and analyse different life stages of parasites over time and in
428 response to perturbation, for example, drug treatment exposure. Whereas scRNA-seq
429 typically requires the rapid processing of fresh tissue and live cells after recovery through to
430 library preparation, snRNA-seq enables sample preservation via freezing, allowing the
431 collection of samples over time that can be processed together, thus reducing library and
432 sequencing batch effects. Here, we demonstrated the versatility of the protocol by sampling
433 multiple species and life stages, each derived from different hosts (*H. contortus* in sheep and
434 *T. muris* from mice) and sampling strategies (invasive and non-invasive sampling from
435 hosts). Moreover, the freezing of parasites enabled sample collection and shipment from
436 geographically distant collaborators rather than having to be physically located with the
437 specimens at the time of collection for immediate processing. Such an approach opens up
438 the possibility of sampling other non-model organisms from diverse or difficult-to-access
439 locations worldwide, provided they can be frozen shortly after collection. The second reason
440 for a nuclei-focused approach is the challenge of tissue dissociation into living cells. Both
441 scRNA-seq and snRNA-seq aim to mirror the transcriptome of cells in tissue, and thus, the
442 recovery of "healthy" cells is paramount. However, stress caused by a combination of
443 physical and/or enzymatic treatment, temperature, and time can alter transcriptional profiles
444 and result in artefacts during data analysis [29,30]. Therefore, effective cellular
445 disassociation of an organism or tissue for scRNA-seq requires a balance between sufficient
446 effort (physical or enzymatic) to disassociate and sufficient care not to damage cells or
447 nuclei so they can be processed. The dissociation of frozen tissue to collect nuclei, in which

448 transcriptional profiles are less susceptible to change and therefore better reflect the
449 transcriptome signature of the cells, can be preferred for difficult-to-dissociate tissues that
450 require greater physical forces to be applied during disassociation. We anticipated this to be
451 important for dissociating parasitic nematodes, many of which are protected by a strong
452 acellular cuticle and sheath and can be very resistant to breaking. Furthermore, our
453 optimised protocol significantly improved the disassociation time; the original protocols
454 tested took ~40-45 minutes to complete, whereas the optimised protocol took ~25 minutes.
455 Other advantages of snRNA-seq over scRNA-seq include the capture of a greater diversity
456 of cell types [31], likely due to differential susceptibility to damage between cell types, and
457 the physical constraints of cell size of commonly used microfluidic technologies, for example,
458 10X Genomics has a recommended maximum cell size limit of 30 µm and a maximum
459 physical microfluidic channel width of 50-60 µm. Cell sizes are known to vary significantly in
460 nematodes; for example, during the development of the model free-living nematode *C.*
461 *elegans*, the intestine significantly increases in tissue volume through to adulthood primarily
462 due to intestinal cells growing in size, becoming multinucleated and polyploid, rather than a
463 large increase in cell number by cell division [26]. We anticipate similar cell-size variation in
464 the closely related *H. contortus* and may equally apply to specialised tissues such as the
465 elongated stichosome of *T. muris* [32]. Moreover, approximately 30% of *C. elegans* somatic
466 nuclei are contained in large, multinucleated cells due to cellular fusion during development
467 to form complex tissues [33]. Due to their unusual cell morphology properties, these cell
468 types will likely be better represented in snRNA-seq than in scRNA-seq data.
469
470 We overcame several challenges during protocol development. For adult stages of parasitic
471 worms, we found that chopping frozen tissue in a single tube on dry ice resulted in more
472 efficient disassociation and lysis than thawing and mincing tissue. However, dissociating
473 microscopic *H. contortus* L3 larvae, an environmentally robust free-living life stage with a
474 sheath surrounding its external cuticle [34], proved more challenging. We explored several
475 approaches, including a *C. elegans* nuclei isolation protocol by Cao *et al.* [35] that used
476 shearing forces from pipetting samples through a 21 G needle for initial tissue disruption.
477 However, in our hands, the *H. contortus* L3 larvae did not shear, whereas the larger adult
478 stages persistently clogged the needle. Our approach of pre-grinding frozen L3 with a
479 porcelain mortar and pestle, followed by a combination of loose and tight Douce strokes and
480 recovery of nuclei in between sets of strokes, improved nuclei recovery significantly.
481 Throughout the protocol, nuclei were lost at each step. We tackled this by recovering nuclei
482 during homogenisation in stages, which prevented excessive mechanical damage and thus
483 maximised the collection of intact nuclei. Once collected, nuclei needed to undergo filtration
484 to remove large and small debris; we found that a single wash step and a 30 µm filter with a

filter wash removes sufficient small and large debris to prevent clogging of the FACS machine capillaries while minimising nuclei loss. The Celegans protocol recommended using Flowmi Cell Strainers, which attach directly to a pipette; however, we found they were easily clogged by the amount of debris in parasitic nematode nuclei suspensions and could not be easily washed to increase nuclei recovery. Furthermore, while FACS removes small debris, reveals diverse nuclei populations, and provides another count measurement, it can also lead to loss of nuclei and decreased nuclei quality [36]. The use of FACS as a filtration step may depend on the degree of debris, and may be worth comparing nuclei for sequencing with and without FACS if debris is minimal. We also experienced nuclei loss during the fixation process of the Parse Biosciences Evercode protocol for snRNA-seq. Parse Biosciences recommends that high nuclei numbers be fixed to account for loss [37]; however, the loss seems sample-dependent and fixation requires optimisation to minimise its impact. For example, the *T. muris* adult male nuclei suspension had a 69.33% nuclei loss vs only 11.88% for *T. muris* adult female samples. This result suggests that some nuclei are more fragile or could be indicative of more extensive nuclear blebbing in the *T. muris* male nuclei, causing an already compromised nuclear envelope to lyse during fixation [38]. Similarly, the Parse Biosciences WT Mini library preparation requires high sample inputs (~55,000 cells/nuclei) at particular concentrations (between 298 and 3,575 cells/nuclei per µL as determined by the number of samples), which can be challenging to achieve with low biomass samples. One potential solution is to combine and concentrate fixed nuclei samples to obtain the proper input concentration, with the caveat that it can result in significant overall nuclei loss due to additional centrifugation and resuspension.

We acknowledge several limitations to our study. While we have gained insights from the two specific parasitic nematode species tested, nuclei isolations from other species (and extension to other non-model organisms) may present their own challenges and require species-specific optimisation, specifically in regard to the number of Dounce tissue grinder strokes. Some variation in nuclei counts may be due to differences in the susceptibility or resistance of some tissues and cell types to disruption. Until more dense atlases are created and a better understanding of cellular/nuclei proportions is made, this is difficult to address. We used Parse Biosciences for library preparation to enable the storage and simultaneous processing of different samples across life stages. However, as described above, the fixation and thawing lead to considerable nuclei loss. If individual or few samples can be processed without freezing and thawing after fixation, higher nuclei counts and more input material for library prep will likely be achieved.

520 # Conclusions

521 We have built on existing approaches to develop an optimised protocol for single nuclei
522 isolation of parasitic nematodes for snRNA-seq. Validation on several diverse species and
523 multiple life stages demonstrates versatility, and critical evaluation of crucial steps enables a
524 significant head-start for using this protocol to isolate nuclei from other non-model
525 organisms. The increasing accessibility of cellular-resolution techniques and optimised
526 protocols will advance the understanding of organisms, such as parasitic nematodes, from
527 fundamental biology to infection and disease, and toward novel approaches to control them.

528 ## Materials and Methods

529 ### *Trichuris muris*

530 #### Mice

531 NSG (NOD.Cg-*Prkdcscid Il2rgtm1Wjl*/SzJ) mice were maintained under specific pathogen-
532 free conditions, under a 12 h light/dark cycle at a temperature of 19-24°C and humidity
533 between 40 and 65%. Mice were fed a regular autoclaved chow diet (LabDiet) and had *ad*
534 *libitum* access to food and water. All efforts were made to minimise suffering through
535 considerate housing and husbandry. Animal welfare was assessed routinely for all mice
536 involved. Mice were naive before the studies described here.
537 Experiments were performed under the regulation of the UK Animals Scientific
538 Procedures Act 1986 under the Project license P77E8A062 and were approved by the
539 Wellcome Sanger Institute Animal Welfare and Ethical Review Body.

540 #### Infection and egg collection

541 Infection and maintenance of *T. muris* were conducted as described [39]. Briefly, NSG mice
542 (6-8 weeks old) were orally infected under anaesthesia with isoflurane with a high dose of
543 embryonated eggs (n = 400) from *T. muris* E-isolate. Mice were monitored daily for general
544 condition and weight loss. Thirty-five days later, mice were culled by cervical dislocation and
545 the caecum and proximal colon were removed. The caecum was split and washed in RPMI-
546 1640 supplemented with 500 U/mL penicillin and 500 µg/mL streptomycin (all from Gibco,
547 UK). Worms were removed using fine forceps and cultured for 4 h or overnight in RPMI-
548 1640/penicillin/streptomycin at 37°C, 5% CO_2. The excretory/secretory (E/S) products from
549 the worm culture were centrifuged (720 *g*, 10 min, room temperature (RT)) to pellet the eggs.
550 The eggs were allowed to embryonate for eight weeks in distilled water in the dark at RT
551 [40,41], and infectivity was established by worm burden in NSG mice.

552 #### Adult worm collection

553 Thirty-five days post-infection, mice were culled by cervical dislocation and the caecum and
554 proximal colon were removed. The caecum was split and washed in RPMI-
555 1640/penicillin/streptomycin. Worms were removed using fine forceps, and males and
556 females were sorted into separate 1.5 mL nuclease-free microcentrifuge tubes. All liquid was
557 removed from the worms in the tubes, and the tubes were submerged in liquid nitrogen and
558 stored at -80°C.
559

Haemonchus contortus

Sheep

Sheep used for experimental infections of *H. contortus* were born and raised under worm free conditions at the Moredun Research Institute, UK. Sheep were humanely euthanased under Schedule 1 of the Animals (Scientific Procedures) Act.

All experimental procedures were examined and approved by the Moredun Research Institute Animal Welfare and Ethics Review Board and were conducted under approved UK Home Office licenses (PPL 60/03899, experimental code identifier E46/11) following the Animals (Scientific Procedures) Act of 1986.

Sheep were infected *Per Os* with 5,000 *H. contortus* MHco3(ISE) L3.

Culturing and collection of L3 larvae

Faeces were collected from 21 days post-infection and coprocultured for 14 days to allow development from egg to L3, after which the larvae were recovered using the Baermann technique before storage at approximately 8°C in tap water. To collect the larvae, water containing the larvae was vacuum filtered through a 10 µm cell strainer (pluriSelect 43-50010-03) fitted to a 250 mL filter flask and washed with 50 mL 1x M9 buffer. Larvae were scraped off the cell strainer using a micro spatula (Fisherbrand 11523482), put in a 1.5 mL nuclease-free microcentrifuge tube, immediately submerged in liquid nitrogen, and stored at -80°C.

Adult worm collection

Adult worms were collected from the abomasum of sheep at necropsy 28 days post-infection. Worms were rinsed in physiological saline (0.85% NaCl) and sexed based on morphology, before male and female adults were sorted into separate 1.5 mL nuclease-free microcentrifuge tubes using a needle. The tubes were submerged in liquid nitrogen and stored at -80°C.

Original single nuclei isolation protocols

Frankenstein

The Frankenstein protocol [20] combines strategies of five protocols for nuclei isolation from mammalian brain tissue [42–46]. First, tissue is minced/chopped with a razor blade on wet

591 ice and added to chilled Nuclei EZ Lysis Buffer in a 1.5 mL tube. A plastic pestle is used to
592 homogenise the sample, and gentle mixing with a wide-bore pipette tip facilitates tissue
593 dissociation. The homogenate is then filtered and washed twice with 1% BSA-PBS. After
594 resuspension in 1% BSA-PBS, the nuclei are filtered through a 35 µm cell strainer and
595 sorted using FACS.

596 Celegans

597 The protocol for single-nuclei isolation from the free-living nematode *C. elegans* originates
598 from a publication by Truong et al. [17]. A 30 µL compact pellet of worms is homogenised in
599 FA cell lysis buffer by applying ten strokes of the tight Dounce tissue grinder pestle in a glass
600 Dounce tissue grinder tube. Further homogenisation is performed using ten strokes with a
601 disposable pellet pestle. Homogenisation with the disposable pellet pestle is repeated twice
602 for a total of 20 strokes. After each set of pestle strokes, the supernatant is collected and
603 centrifuged at low speed to pellet large debris. The nuclei in suspension are pelleted,
604 washed with 1% BSA-PBS, and filtered using a 40 µm Flowmi tip filter. Filtered nuclei were
605 sorted using FACS.

606 Human Cell Atlas (HCA)

607 The protocol used by the Human Cell Atlas team at the Wellcome Sanger Institute [19] is
608 adapted from the protocol by Nadelmann et al. [47]. The tissue sample is not minced or
609 chopped before placing it in a glass Dounce tissue grinder tube with a homemade
610 homogenisation buffer. A protease inhibitor is recommended to be included in the
611 homogenisation buffer, but we did not include it because it is only necessary for proteomics.
612 The tissue is homogenised with 10-20 strokes using the loose Dounce tissue grinder pestle
613 until no resistance is felt. The tight Dounce tissue grinder pestle is then applied 10-20 times
614 until no resistance is felt. The homogenate is filtered through a 40 µm cell strainer and
615 washed once with 5% BSA-PBS wash buffer. An optional gradient centrifugation step is
616 described using Lymphoprep or Percoll to remove debris.

617 An optimised protocol for nematode single nuclei isolation

618 A detailed, step-by-step protocol is available on STAR Protocols. All reagents and
619 equipment are pre-chilled on wet ice unless otherwise stated. Twenty adult female *H.*
620 *contortus* worms were cut into pieces <2 mm while on dry ice using spring scissors pre-
621 chilled in a 50 mL Falcon tube on dry ice. The tissue is placed in a 1 mL Wheaton Dounce
622 tissue grinder (DWK Life Sciences) containing 500 µL Nuclei EZ Lysis Buffer (Sigma-Aldrich)
623 with the addition of 25 µg/mL DNase I, 5 mM $MgCl_2$, and 0.2 U/µL SUPERase In RNase
624 inhibitor using a glass Dounce tissue grinder. The loose Dounce tissue grinder pestle is

625 applied five times, followed by three strokes of the tight Dounce tissue grinder pestle. The
626 homogenate is incubated on ice for up to 4 min or until the large undissociated tissue and
627 debris settle. The supernatant containing the nuclei is collected in a 5 mL Protein LoBind
628 tube (Eppendorf). Fresh lysis buffer is added to the Dounce to replace the removed
629 supernatant. Three additional strokes of the tight Dounce tissue grinder pestle are applied,
630 followed by incubation and supernatant collection. Homogenisation with the tight Dounce
631 tissue grinder pestle is repeated up to three more times or until the settled homogenate is
632 clear. The nuclei are pelleted, washed once with 2% BSA-PBS wash buffer containing 0.2
633 U/µL SUPERase·In (ThermoFisher) and 5 mM EDTA, and filtered using a 30 µm CellTrics
634 filter (Sysmex). Nuclei isolation should take no more than 30 min. The filter is washed with
635 additional wash buffer to maximise the recovery of nuclei. Nuclei are sorted using FACS to
636 remove small debris.

637

638 ### Flow cytometry and Fluorescence-Activated Cell Sorting (FACS)

639 The Bigfoot Spectral Cell Sorter (ThermoFisher) was used to assess and sort nuclei. A 50
640 µL aliquot of nuclei from each sample was used as a negative control for fluorescent staining
641 detection levels. The remaining sample (~500 µL) was stained with 5 µL 1,000x SYBR
642 Green I (ThermoFisher) for sorting. Flow cytometry was performed using the 488 nm laser
643 and 507/19 filter. For this study, nuclei were gated only on a positive SYBR Green I signal
644 (**Supplementary Figure 3**) to avoid omitting the unusually small and large nuclei observed
645 in microscopy. Nuclei were collected in pre-chilled 1% BSA-blocked 5 mL Protein LoBind
646 tube (Eppendorf) containing the 2% BSA-PBS wash buffer detailed above and kept on ice.

647

648 ### Sample fixation

649 After sorting, the nuclei concentration was determined using a C-Chip disposable
650 hemocytometer (NanoEntek). The nuclei suspension was centrifuged for 10 mins at 500 g
651 and 4°C. The Evercode Nuclei Fixation kit (Parse Biosciences) with user manual v2.0.2 was
652 used with the following modifications. The 15 mL polypropylene tubes were replaced with
653 1% BSA-blocked 5 mL Protein LoBind tubes (Eppendorf). Briefly, tubes were filled with 1%
654 BSA-NFW solution, incubated for 30 mins at room temperature, and then dried in a laminar
655 flow cabinet. All centrifugation steps were done at 500 g. Because our nuclei suspensions
656 were fairly dilute (~100,000 nuclei starting) and nuclei clumping was not observed, we
657 skipped the two 40 µm straining steps in the fixation protocol to maximise nuclei retention.

658 Also, because of the low concentration, nuclei were resuspended in only 50 µL Nuclei
659 Buffer, and the DMSO concentration was adjusted proportionally. Fixed nuclei were placed
660 in a Corning CoolCell Cell Freezing container and stored at -80°C until all nuclei
661 preparations were collected. Fixed nuclei can be stored for up to 6 months.

662

663 ## Library preparation and sequencing

664 Combinatorial barcoding, cDNA amplification, and library preparation were performed using
665 the Evercode WT Mini v2 kits (Parse Biosciences) and user manual v2.0.1. A 10 µL aliquot
666 of fixed nuclei from each sample's nuclei suspension is thawed at 37°C, and nuclei are
667 manually counted using a C-Chip haemocytometer. Nuclei concentrations are input into the
668 "Parse Biosciences Evercode WT Mini Sample Loading Table V1.2.0", and the amount of
669 sample stock needed is automatically calculated per the user's specific sample number, the
670 desired number of barcoded cells, and the percentage of the library that is represented by
671 each sample. Samples are allocated into specific wells according to the Sample Loading
672 Table. First, sample-specific barcodes are applied to the nuclei, and reverse transcription
673 takes place. Nuclei from all wells are then pooled and redistributed across a second plate
674 that contains a second barcode. Nuclei are pooled and split on a third plate to add a third
675 barcode. After ligating three total barcodes, nuclei are pooled and counted manually using a
676 C-Chip haemocytometer. Barcoded nuclei can be split into multiple sublibraries according to
677 user needs. We performed seven cycles in the second cDNA amplification step and thirteen
678 cycles in the sublibrary index amplification PCR, according to kit specifications. We
679 performed seven cycles in the second cDNA amplification step and ten cycles in the
680 sublibrary index amplification PCR, according to kit specifications. Nuclei in the sublibraries
681 are then lysed, and a fourth, sublibrary-specific barcode is added by PCR extension. Library
682 preparation adds Illumina-compatible adapters for loading onto a sequencer. The HS D5000
683 Tapestation assay was used for fragment analysis of the cDNA sublibraries and final
684 libraries for sequencing. The HS dsDNA Qubit assay was used to quantify the sublibraries
685 and final libraries. The cDNA fragment analyses for the sublibraries and final libraries are
686 shown in **Supplementary Figure 3**.
687
688 The resulting libraries were combined with 5% PhiX before sequencing each library on an
689 Illumina NovaSeq 6000 lane using 150 bp paired-end reads, generating 316,638,084 and
690 307,516,986 reads for Library 1 and Library 2, respectively.
691

Single nuclei RNA-seq analysis

Raw sequencing data were first assessed using FastQC (v0.12.1) (https://www.bioinformatics.babraham.ac.uk/projects/fastqc/) and MultiQC (v1.17) [48] before analysis using the Parse Biosciences split-pipe (v1.1.2) pipeline. Reference genomes and annotations were downloaded from WormBase ParaSite for *H. contortus* (PRJEB506 [49]) and *T. muris* (PRJEB126 [50]). Reference databases for each species were created using *split-pipe --mode mkref* incorporating both genome (fasta) and annotation (gtf) before raw reads were mapped to each reference database using split-pipe --mode all (parfile: post_min_map_frac 0.01). Mapping statistics, including reads mapped, nuclei identified, and the number of genes and transcripts per nuclei, were collated and visualised from the resulting HTML reports.

Further analysis, including nuclei cluster identification based on differentially expressed transcripts, generation of UMAP plots, and exploration of cluster identity based on marker genes, was performed in R (v4.1.3) using Seurat v5 [51]. UMAPs were visualised, combining all life stages per species and subsequently coloured by life stage or cluster ID. Expression of select genes to highlight cluster specificity and identity was visualised using Seurat *FeaturePlot.* To infer the biological relevance or putative tissue type of each cluster, the top 20 differentially expressed genes per cluster were obtained, from which the *C. elegans* orthologs were identified using WormBase ParaSite Biomart [52]. Functional enrichment was performed using the *C. elegans* orthologs and the web platform WormEnrichr [53,54]. The parasite genes were also assessed using species-specific GO terms using g:Profiler (version e111_eg58_p18_f463989d) [55].

Code and data availability

Reference genomes and annotations used in the analysis can be accessed from WormBase ParaSite (https://parasite.wormbase.org/). Raw sequencing data can be accessed from the European Nucleotide Archive (ENA) under the study accession ERP140984. The code used to analyse sequencing data can be accessed from https://github.com/stephenrdoyle/single_cell_optimisation. Any additional information required to reanalyse the data reported in this paper is available from one of the lead contacts.

Acknowledgements

We gratefully acknowledge the technical support and advice of Ian Pittam from Parse Biosciences, the Pathogen Informatics group at the Wellcome Sanger Institute for informatics support, and the Helminth Genomics group at the Wellcome Sanger Institute for constructive feedback on the analyses and manuscript.

This work is supported by a UKRI Future Leaders Fellowship to SRD [MR/T020733/1] and the Wellcome Trust (UK) through core funding to the Wellcome Sanger Institute (UK) [206194]. AAM and DJB receive underpinning national capacity funding from the Rural and Environment Science and Analytical Services (RESAS) division of the Scottish Government. M.A.D-C was supported by the Sir Henry Dale Fellowship jointly funded by the Wellcome Trust and the Royal Society (222546/Z/21/Z); the Wellcome Trust (203151/Z/16/Z, 203151/A/16/Z) and the UKRI Medical Research Council (MC_PC_17230). For the purpose of Open Access, the author has applied a CC BY public copyright licence to any Author Accepted Manuscript version arising from this submission.

References

1. Howick VM, Russell AJC, Andrews T, Heaton H, Reid AJ, Natarajan K, et al. The Malaria Cell Atlas: Single parasite transcriptomes across the complete *Plasmodium* life cycle. Science. 2019;365. Available from: http://dx.doi.org/10.1126/science.aaw2619

2. Real E, Howick VM, Dahalan FA, Witmer K, Cudini J, Andradi-Brown C, et al. A single-cell atlas of *Plasmodium falciparum* transmission through the mosquito. Nat Commun. 2021;12:3196. Available from: http://dx.doi.org/10.1038/s41467-021-23434-z

3. Reid AJ, Talman AM, Bennett HM, Gomes AR, Sanders MJ, Illingworth CJR, et al. Single-cell RNA-seq reveals hidden transcriptional variation in malaria parasites. Elife. 2018;7. Available from: http://dx.doi.org/10.7554/eLife.33105

4. Howick VM, Peacock L, Kay C, Collett C, Gibson W, Lawniczak MKN. Single-cell transcriptomics reveals expression profiles of *Trypanosoma brucei* sexual stages. PLoS Pathog. 2022;18:e1010346. Available from: http://dx.doi.org/10.1371/journal.ppat.1010346

5. Briggs EM, Rojas F, McCulloch R, Matthews KR, Otto TD. Single-cell transcriptomic analysis of bloodstream *Trypanosoma brucei* reconstructs cell cycle progression and developmental quorum sensing. Nat Commun. 2021;12:5268. Available from: http://dx.doi.org/10.1038/s41467-021-25607-2

6. Vigneron A, O'Neill MB, Weiss BL, Savage AF, Campbell OC, Kamhawi S, et al. Single-cell RNA sequencing of from tsetse salivary glands unveils metacyclogenesis and identifies potential transmission blocking antigens. Proc Natl Acad Sci U S A. 2020;117:2613–21. Available from: http://dx.doi.org/10.1073/pnas.1914423117

7. Briggs EM, Marques CA, Oldrieve GR, Hu J, Otto TD, Matthews KR. Profiling the bloodstream form and procyclic form cell cycle using single-cell transcriptomics. Elife. 2023;12. Available from: http://dx.doi.org/10.7554/eLife.86325

8. Diaz Soria CL, Lee J, Chong T, Coghlan A, Tracey A, Young MD, et al. Single-cell atlas of the first intra-mammalian developmental stage of the human parasite *Schistosoma mansoni*. Nat Commun. 2020;11:6411. Available from: http://dx.doi.org/10.1038/s41467-020-20092-5

9. Li P, Nanes Sarfati D, Xue Y, Yu X, Tarashansky AJ, Quake SR, et al. Single-cell analysis of *Schistosoma mansoni* identifies a conserved genetic program controlling germline stem cell fate. Nat Commun. 2021;12:485. Available from: http://dx.doi.org/10.1038/s41467-020-20794-w

10. Attenborough T, Rawlinson KA, Diaz Soria CL, Ambridge K, Sankaranarayanan G, Graham J, et al. A single-cell atlas of the miracidium larva of reveals cell types, developmental pathways, and tissue architecture. Elife. 2024;13. Available from: http://dx.doi.org/10.7554/eLife.95628

11. Diaz Soria CL, Attenborough T, Lu Z, Fontenla S, Graham J, Hall C, et al. Single-cell transcriptomics of the human parasite *Schistosoma mansoni* first intra-molluscan stage reveals tentative tegumental and stem-cell regulators. Sci Rep. 2024;14:5974. Available from: http://dx.doi.org/10.1038/s41598-024-55790-3

12. Puckelwaldt O, Gramberg S, Ajmera S, Koepke J, Samakovlis C, Haeberlein S. Single-cell transcriptomics identifies a p21-activated kinase important for survival of the zoonotic parasite *Fasciola hepatica*. bioRxiv. 2024 [cited 2024 Oct 21]. p. 2024.03.26.586785. Available from: https://www.biorxiv.org/content/10.1101/2024.03.26.586785v1.abstract

13. Henthorn CR, Airs PM, Neumann EK, Zamanian M. Resolving the origins of secretory products and anthelmintic responses in a human parasitic nematode at single-cell resolution. Elife. 2023;12. Available from: http://dx.doi.org/10.7554/eLife.83100

14. Tyagi R, Rosa BA, Swain A, Artyomov MN, Jasmer DP, Mitreva M. Intestinal cell diversity and treatment responses in a parasitic nematode at single cell resolution. BMC Genomics. 2024 [cited 2024 Sep 25];25:1–21. Available from: https://link.springer.com/articles/10.1186/s12864-024-10203-7

15. Korhonen PK, Wang T, Young ND, Byrne JJ, Campos TL, Chang BCH, et al. Analysis of Haemonchus embryos at single cell resolution identifies two eukaryotic elongation factors as intervention target candidates. Comput Struct Biotechnol J. 2024;23:1026–35. Available from: https://pubmed.ncbi.nlm.nih.gov/38435301/

16. Pollo SMJ, Liu H, Coria AL, Rosin N, Labit E, Biernaskie J, et al. A single-cell transcriptomics atlas for the parasitic nematode *Heligmosomoides bakeri*: Extrapolating model organism information to non-model systems. bioRxiv. 2024. Available from: http://biorxiv.org/lookup/doi/10.1101/2024.02.27.582282

17. Truong L, Chen Y-W, Barrere-Cain R, Levenson MT, Shuck K, Xiao W, et al. Single-nucleus resolution mapping of the adult *C. elegans* and its application to elucidate inter- and trans-generational response to alcohol. Cell Rep. 2023 [cited 2024 Jul 4];42. Available from: http://www.cell.com/article/S2211124723005466/abstract

18. Levenson MT, Barrere-Cain R, Truong L, Chen Y-W, Shuck K, Panter B, et al. Protocol for nuclear dissociation of the adult *C. elegans* for single-nucleus RNA sequencing and its application for mapping environmental responses. STAR Protocols. 2023 [cited 2024 Oct 21];4:102756. Available from: http://dx.doi.org/10.1016/j.xpro.2023.102756

19. Stephenson E. Nuclei isolation from frozen tissue. protocols.io; 2023 Jun. Available from: https://www.protocols.io/view/nuclei-isolation-from-frozen-tissue-cwcmxau6

20. G Martelotto L, Martelotto L. “Frankenstein” protocol for nuclei isolation from fresh and frozen tissue for snRNAseq v3. protocols.io. ZappyLab, Inc.; 2020. Available from: https://www.protocols.io/view/frankenstein-protocol-for-nuclei-isolation-from-f-bqxymxpw

21. Regev A, Teichmann SA, Lander ES, Amit I, Benoist C, Birney E, et al. The Human Cell Atlas. Elife. 2017 [cited 2024 Oct 20];6. Available from: https://pubmed.ncbi.nlm.nih.gov/29206104/

22. Best Practices to Minimize Chromium Next GEM Chip Clogs and Wetting Failures. 10x Genomics; 2022. Report No.: CG000479 Rev B. Available from: https://cdn.10xgenomics.com/image/upload/v1660261285/support-documents/CG000479_TechNote_MinimizingClogs_WettingFailures_RevB.pdf

23. Madissoon E, Wilbrey-Clark A, Miragaia RJ, Saeb-Parsy K, Mahbubani KT, Georgakopoulos N, et al. scRNA-seq assessment of the human lung, spleen, and esophagus tissue stability after cold preservation. Genome Biol. 2019;21:1. Available from: http://dx.doi.org/10.1186/s13059-019-1906-x

24. Can I use an alternative RNase inhibitor part number?. 10x Genomics; Available from: https://kb.10xgenomics.com/hc/en-us/articles/360049543672-Can-I-use-an-alternative-RNase-inhibitor-part-number

25. International Helminth Genomes Consortium. Comparative genomics of the major parasitic worms. Nat Genet. 2018;51:163–74. Available from:

828 http://dx.doi.org/10.1038/s41588-018-0262-1

829 26. Hedgecock EM, White JG. Polyploid tissues in the nematode *Caenorhabditis elegans*.
830 Dev Biol. 1985;107:128–33. Available from: http://dx.doi.org/10.1016/0012-1606(85)90381-1

831 27. Rosenberg AB, Roco CM, Muscat RA, Kuchina A, Sample P, Yao Z, et al. Single-cell
832 profiling of the developing mouse brain and spinal cord with split-pool barcoding. Science.
833 2018;360:176–82. Available from: http://dx.doi.org/10.1126/science.aam8999

834 28. Doyle SR. Improving helminth genome resources in the post-genomic era. Trends
835 Parasitol. 2022;38:831–40. Available from: http://dx.doi.org/10.1016/j.pt.2022.06.002

836 29. Wu H, Kirita Y, Donnelly EL, Humphreys BD. Advantages of Single-Nucleus over Single-
837 Cell RNA Sequencing of Adult Kidney: Rare Cell Types and Novel Cell States Revealed in
838 Fibrosis. J Am Soc Nephrol. 2019;30:23–32. Available from:
839 http://dx.doi.org/10.1681/ASN.2018090912

840 30. van den Brink SC, Sage F, Vértesy Á, Spanjaard B, Peterson-Maduro J, Baron CS, et al.
841 Single-cell sequencing reveals dissociation-induced gene expression in tissue
842 subpopulations. Nat Methods. 2017 [cited 2024 Oct 10];14:935–6. Available from:
843 https://www.nature.com/articles/nmeth.4437

844 31. Slyper M, Porter CBM, Ashenberg O, Waldman J, Drokhlyansky E, Wakiro I, et al. A
845 single-cell and single-nucleus RNA-Seq toolbox for fresh and frozen human tumors. Nat
846 Med. 2020;26:792–802. Available from: http://dx.doi.org/10.1038/s41591-020-0844-1

847 32. O'Sullivan JDB, Cruickshank SM, Withers PJ, Else KJ. Morphological variability in the
848 mucosal attachment site of *Trichuris muris* revealed by X-ray microcomputed tomography.
849 Int J Parasitol. 2021;51:797–807. Available from:
850 http://dx.doi.org/10.1016/j.ijpara.2021.04.006

851 33. Podbilewicz B. Cell fusion. In: Kramer JM, Moerman DG, editors. WormBook: The online
852 review of C elegans biology. The C. elegans Research Community; 2006 [cited 2024 Nov 7].
853 Available from: http://www.wormbook.org/chapters/www_cellfusion/cellfusion.html#bib57

854 34. Cantacessi C, Campbell BE, Young ND, Jex AR, Hall RS, Presidente PJA, et al.
855 Differences in transcription between free-living and CO2-activated third-stage larvae of
856 *Haemonchus contortus*. BMC Genomics. 2010;11:266. Available from:
857 http://dx.doi.org/10.1186/1471-2164-11-266

858 35. Cao J, Packer JS, Ramani V, Cusanovich DA, Huynh C, Daza R, et al. Comprehensive
859 single-cell transcriptional profiling of a multicellular organism. Science. 2017;357:661–7.
860 Available from: http://dx.doi.org/10.1126/science.aam8940

861 36. Alfieri JM, Wang G, Jonika MM, Gill CA, Blackmon H, Athrey GN. A Primer for Single-
862 Cell Sequencing in Non-Model Organisms. Genes. 2022;13. Available from:
863 http://dx.doi.org/10.3390/genes13020380

864 37. Evercode Fixation and WT v2 User Guides. Parse Biosciences; 2023. Available from:
865 https://support.parsebiosciences.com/hc/en-us/articles/23915040729876-Evercode-Fixation-
866 and-WT-v2-User-Guides

867 38. Srivastava N, Nader GP de F, Williart A, Rollin R, Cuvelier D, Lomakin A, et al. Nuclear
868 fragility, blaming the blebs. Curr Opin Cell Biol. 2021;70:100–8. Available from:
869 https://pubmed.ncbi.nlm.nih.gov/33662810/

870 39. Wakelin D. Acquired immunity to *Trichuris muris* in the albino laboratory mouse.
871 Parasitology. 1967;57:515–24. Available from:
872 http://dx.doi.org/10.1017/s0031182000072395

873 40. White EC, Houlden A, Bancroft AJ, Hayes KS, Goldrick M, Grencis RK, et al.
874 Manipulation of host and parasite microbiotas: Survival strategies during chronic nematode
875 infection. Sci Adv. 2018;4:eaap7399. Available from:
876 http://dx.doi.org/10.1126/sciadv.aap7399

877 41. Duque-Correa MA, Karp NA, McCarthy C, Forman S, Goulding D, Sankaranarayanan G,
878 et al. Exclusive dependence of IL-10Rα signalling on intestinal microbiota homeostasis and
879 control of whipworm infection. PLoS Pathog. 2019;15:e1007265. Available from:
880 http://dx.doi.org/10.1371/journal.ppat.1007265

881 42. Hu P, Fabyanic E, Kwon DY, Tang S, Zhou Z, Wu H. Dissecting Cell-Type Composition
882 and Activity-Dependent Transcriptional State in Mammalian Brains by Massively Parallel
883 Single-Nucleus RNA-Seq. Mol Cell. 2017;68:1006–15.e7. Available from:
884 http://dx.doi.org/10.1016/j.molcel.2017.11.017

885 43. Habib N, Li Y, Heidenreich M, Swiech L, Avraham-Davidi I, Trombetta JJ, et al. Div-Seq:
886 Single-nucleus RNA-Seq reveals dynamics of rare adult newborn neurons. Science.
887 2016;353:925–8. Available from: http://dx.doi.org/10.1126/science.aad7038

888 44. Habib N, Avraham-Davidi I, Basu A, Burks T, Shekhar K, Hofree M, et al. Massively
889 parallel single-nucleus RNA-seq with DroNc-seq. Nat Methods. 2017;14:955–8. Available
890 from: http://dx.doi.org/10.1038/nmeth.4407

891 45. Lake BB, Ai R, Kaeser GE, Salathia NS, Yung YC, Liu R, et al. Neuronal subtypes and
892 diversity revealed by single-nucleus RNA sequencing of the human brain. Science.
893 2016;352:1586–90. Available from: http://dx.doi.org/10.1126/science.aaf1204

894 46. Lacar B, Linker SB, Jaeger BN, Krishnaswami S, Barron J, Kelder M, et al. Nuclear
895 RNA-seq of single neurons reveals molecular signatures of activation. Nat Commun.
896 2016;7:11022. Available from: https://www.nature.com/articles/ncomms11022

897 47. Nadelmann ER, Gorham JM, Reichart D, Delaughter DM, Wakimoto H, Lindberg EL, et
898 al. Isolation of Nuclei from Mammalian Cells and Tissues for Single-Nucleus Molecular
899 Profiling. Curr Protoc. 2021;1:e132. Available from: http://dx.doi.org/10.1002/cpz1.132

900 48. Ewels P, Magnusson M, Lundin S, Käller M. MultiQC: summarize analysis results for
901 multiple tools and samples in a single report. Bioinformatics. 2016;32:3047–8. Available
902 from: http://dx.doi.org/10.1093/bioinformatics/btw354

903 49. Doyle SR, Tracey A, Laing R, Holroyd N, Bartley D, Bazant W, et al. Genomic and
904 transcriptomic variation defines the chromosome-scale assembly of *Haemonchus contortus*,
905 a model gastrointestinal worm. Commun Biol. 2020;3:656. Available from:
906 http://dx.doi.org/10.1038/s42003-020-01377-3

907 50. Foth BJ, Tsai IJ, Reid AJ, Bancroft AJ, Nichol S, Tracey A, et al. Whipworm genome and
908 dual-species transcriptome analyses provide molecular insights into an intimate host-
909 parasite interaction. Nat Genet. 2014 [cited 2023 Nov 16];46:693–700. Available from:
910 https://www.nature.com/articles/ng.3010

911 51. Hao Y, Stuart T, Kowalski MH, Choudhary S, Hoffman P, Hartman A, et al. Dictionary
912 learning for integrative, multimodal and scalable single-cell analysis. Nat Biotechnol.
913 2024;42:293–304. Available from: https://www.ncbi.nlm.nih.gov/pmc/articles/PMC10928517/

914 52. Howe KL, Bolt BJ, Shafie M, Kersey P, Berriman M. WormBase ParaSite - a
915 comprehensive resource for helminth genomics. Mol Biochem Parasitol. 2017;215:2–10.
916 Available from: http://dx.doi.org/10.1016/j.molbiopara.2016.11.005

917 53. Kuleshov MV, Jones MR, Rouillard AD, Fernandez NF, Duan Q, Wang Z, et al. Enrichr:
918 a comprehensive gene set enrichment analysis web server 2016 update. Nucleic Acids Res.
919 2016;44:W90–7. Available from: http://dx.doi.org/10.1093/nar/gkw377

920 54. Chen EY, Tan CM, Kou Y, Duan Q, Wang Z, Meirelles GV, et al. Enrichr: interactive and
921 collaborative HTML5 gene list enrichment analysis tool. BMC Bioinformatics. 2013;14:128.
922 Available from: http://dx.doi.org/10.1186/1471-2105-14-128

923 55. Kolberg L, Raudvere U, Kuzmin I, Adler P, Vilo J, Peterson H. g:Profiler-interoperable
924 web service for functional enrichment analysis and gene identifier mapping (2023 update).
925 Nucleic Acids Res. 2023;51:W207–12. Available from: http://dx.doi.org/10.1093/nar/gkad347

926 1. Howick VM, Russell AJC, Andrews T, Heaton H, Reid AJ, Natarajan K, et al. The Malaria
927 Cell Atlas: Single parasite transcriptomes across the complete Plasmodium life cycle.
928 Science. 2019;365. Available from: http://dx.doi.org/10.1126/science.aaw2619

929 2. Real E, Howick VM, Dahalan FA, Witmer K, Cudini J, Andradi-Brown C, et al. A single-cell
930 atlas of Plasmodium falciparum transmission through the mosquito. Nat Commun.
931 2021;12:3196. Available from: http://dx.doi.org/10.1038/s41467-021-23434-z

932 3. Reid AJ, Talman AM, Bennett HM, Gomes AR, Sanders MJ, Illingworth CJR, et al. Single-
933 cell RNA-seq reveals hidden transcriptional variation in malaria parasites. Elife. 2018;7.
934 Available from: http://dx.doi.org/10.7554/eLife.33105

935 4. Howick VM, Peacock L, Kay C, Collett C, Gibson W, Lawniczak MKN. Single-cell
936 transcriptomics reveals expression profiles of Trypanosoma brucei sexual stages. PLoS
937 Pathog. 2022;18:e1010346. Available from: http://dx.doi.org/10.1371/journal.ppat.1010346

938 5. Briggs EM, Rojas F, McCulloch R, Matthews KR, Otto TD. Single-cell transcriptomic
939 analysis of bloodstream Trypanosoma brucei reconstructs cell cycle progression and
940 developmental quorum sensing. Nat Commun. 2021;12:5268. Available from:
941 http://dx.doi.org/10.1038/s41467-021-25607-2

942 6. Vigneron A, O'Neill MB, Weiss BL, Savage AF, Campbell OC, Kamhawi S, et al. Single-
943 cell RNA sequencing of from tsetse salivary glands unveils metacyclogenesis and identifies
944 potential transmission blocking antigens. Proc Natl Acad Sci U S A. 2020;117:2613–21.
945 Available from: http://dx.doi.org/10.1073/pnas.1914423117

946 7. Briggs EM, Marques CA, Oldrieve GR, Hu J, Otto TD, Matthews KR. Profiling the
947 bloodstream form and procyclic form cell cycle using single-cell transcriptomics. Elife.
948 2023;12. Available from: http://dx.doi.org/10.7554/eLife.86325

949 8. Diaz Soria CL, Lee J, Chong T, Coghlan A, Tracey A, Young MD, et al. Single-cell atlas of
950 the first intra-mammalian developmental stage of the human parasite Schistosoma mansoni.
951 Nat Commun. 2020;11:6411. Available from: http://dx.doi.org/10.1038/s41467-020-20092-5

952 9. Li P, Nanes Sarfati D, Xue Y, Yu X, Tarashansky AJ, Quake SR, et al. Single-cell analysis
953 of Schistosoma mansoni identifies a conserved genetic program controlling germline stem
954 cell fate. Nat Commun. 2021;12:485. Available from: http://dx.doi.org/10.1038/s41467-020-
955 20794-w

956 10. Attenborough T, Rawlinson KA, Diaz Soria CL, Ambridge K, Sankaranarayanan G,

957 Graham J, et al. A single-cell atlas of the miracidium larva of reveals cell types,
958 developmental pathways, and tissue architecture. Elife. 2024;13. Available from:
959 http://dx.doi.org/10.7554/eLife.95628

960 11. Diaz Soria CL, Attenborough T, Lu Z, Fontenla S, Graham J, Hall C, et al. Single-cell
961 transcriptomics of the human parasite Schistosoma mansoni first intra-molluscan stage
962 reveals tentative tegumental and stem-cell regulators. Sci Rep. 2024;14:5974. Available
963 from: http://dx.doi.org/10.1038/s41598-024-55790-3

964 12. Puckelwaldt O, Gramberg S, Ajmera S, Koepke J, Samakovlis C, Haeberlein S. Single-
965 cell transcriptomics identifies a p21-activated kinase important for survival of the zoonotic
966 parasite Fasciola hepatica. bioRxiv. 2024 [cited 2024 Oct 21]. p. 2024.03.26.586785.
967 Available from: https://www.biorxiv.org/content/10.1101/2024.03.26.586785v1.abstract

968 13. Henthorn CR, Airs PM, Neumann EK, Zamanian M. Resolving the origins of secretory
969 products and anthelmintic responses in a human parasitic nematode at single-cell resolution.
970 Elife. 2023;12. Available from: http://dx.doi.org/10.7554/eLife.83100

971 14. Tyagi R, Rosa BA, Swain A, Artyomov MN, Jasmer DP, Mitreva M. Intestinal cell
972 diversity and treatment responses in a parasitic nematode at single cell resolution. BMC
973 Genomics. 2024 [cited 2024 Sep 25];25:1–21. Available from:
974 https://link.springer.com/articles/10.1186/s12864-024-10203-7

975 15. Korhonen PK, Wang T, Young ND, Byrne JJ, Campos TL, Chang BCH, et al. Analysis of
976 Haemonchus embryos at single cell resolution identifies two eukaryotic elongation factors as
977 intervention target candidates. Comput Struct Biotechnol J. 2024;23:1026–35. Available
978 from: https://pubmed.ncbi.nlm.nih.gov/38435301/

979 16. Pollo SMJ, Liu H, Coria AL, Rosin N, Labit E, Biernaskie J, et al. A single-cell
980 transcriptomics atlas for the parasitic nematode Heligmosomoides bakeri: Extrapolating
981 model organism information to non-model systems. bioRxiv. 2024. Available from:
982 http://biorxiv.org/lookup/doi/10.1101/2024.02.27.582282

983 17. Truong L, Chen Y-W, Barrere-Cain R, Levenson MT, Shuck K, Xiao W, et al. Single-
984 nucleus resolution mapping of the adult C. elegans and its application to elucidate inter- and
985 trans-generational response to alcohol. Cell Rep. 2023 [cited 2024 Jul 4];42. Available from:
986 http://www.cell.com/article/S2211124723005466/abstract

987 18. Levenson MT, Barrere-Cain R, Truong L, Chen Y-W, Shuck K, Panter B, et al. Protocol
988 for nuclear dissociation of the adult C. elegans for single-nucleus RNA sequencing and its
989 application for mapping environmental responses. STAR Protocols. 2023 [cited 2024 Oct
990 21];4:102756. Available from: http://dx.doi.org/10.1016/j.xpro.2023.102756

991 19. Stephenson E. Nuclei isolation from frozen tissue. protocols.io; 2023 Jun. Available from:
992 https://www.protocols.io/view/nuclei-isolation-from-frozen-tissue-cwcmxau6

993 20. G Martelotto L, Martelotto L. “Frankenstein” protocol for nuclei isolation from fresh and
994 frozen tissue for snRNAseq v3. protocols.io. ZappyLab, Inc.; 2020. Available from:
995 https://www.protocols.io/view/frankenstein-protocol-for-nuclei-isolation-from-f-bqxymxpw

996 21. Regev A, Teichmann SA, Lander ES, Amit I, Benoist C, Birney E, et al. The Human Cell
997 Atlas. Elife. 2017 [cited 2024 Oct 20];6. Available from:
998 https://pubmed.ncbi.nlm.nih.gov/29206104/

999 22. Best Practices to Minimize Chromium Next GEM Chip Clogs and Wetting Failures. 10x
1000 Genomics; 2022. Report No.: CG000479 Rev B. Available from:

1001 https://cdn.10xgenomics.com/image/upload/v1660261285/support-
1002 documents/CG000479_TechNote_MinimizingClogs_WettingFailures_RevB.pdf

1003 23. Madissoon E, Wilbrey-Clark A, Miragaia RJ, Saeb-Parsy K, Mahbubani KT,
1004 Georgakopoulos N, et al. scRNA-seq assessment of the human lung, spleen, and
1005 esophagus tissue stability after cold preservation. Genome Biol. 2019;21:1. Available from:
1006 http://dx.doi.org/10.1186/s13059-019-1906-x

1007 24. Can I use an alternative RNase inhibitor part number?. 10x Genomics; Available from:
1008 https://kb.10xgenomics.com/hc/en-us/articles/360049543672-Can-I-use-an-alternative-
1009 RNase-inhibitor-part-number

1010 25. International Helminth Genomes Consortium. Comparative genomics of the major
1011 parasitic worms. Nat Genet. 2018;51:163–74. Available from:
1012 http://dx.doi.org/10.1038/s41588-018-0262-1

1013 26. Hedgecock EM, White JG. Polyploid tissues in the nematode Caenorhabditis elegans.
1014 Dev Biol. 1985;107:128–33. Available from: http://dx.doi.org/10.1016/0012-1606(85)90381-1

1015 27. Rosenberg AB, Roco CM, Muscat RA, Kuchina A, Sample P, Yao Z, et al. Single-cell
1016 profiling of the developing mouse brain and spinal cord with split-pool barcoding. Science.
1017 2018;360:176–82. Available from: http://dx.doi.org/10.1126/science.aam8999

1018 28. Doyle SR. Improving helminth genome resources in the post-genomic era. Trends
1019 Parasitol. 2022;38:831–40. Available from: http://dx.doi.org/10.1016/j.pt.2022.06.002

1020 29. Wu H, Kirita Y, Donnelly EL, Humphreys BD. Advantages of Single-Nucleus over Single-
1021 Cell RNA Sequencing of Adult Kidney: Rare Cell Types and Novel Cell States Revealed in
1022 Fibrosis. J Am Soc Nephrol. 2019;30:23–32. Available from:
1023 http://dx.doi.org/10.1681/ASN.2018090912

1024 30. van den Brink SC, Sage F, Vértesy Á, Spanjaard B, Peterson-Maduro J, Baron CS, et al.
1025 Single-cell sequencing reveals dissociation-induced gene expression in tissue
1026 subpopulations. Nat Methods. 2017 [cited 2024 Oct 10];14:935–6. Available from:
1027 https://www.nature.com/articles/nmeth.4437

1028 31. Slyper M, Porter CBM, Ashenberg O, Waldman J, Drokhlyansky E, Wakiro I, et al. A
1029 single-cell and single-nucleus RNA-Seq toolbox for fresh and frozen human tumors. Nat
1030 Med. 2020;26:792–802. Available from: http://dx.doi.org/10.1038/s41591-020-0844-1

1031 32. O'Sullivan JDB, Cruickshank SM, Withers PJ, Else KJ. Morphological variability in the
1032 mucosal attachment site of Trichuris muris revealed by X-ray microcomputed tomography.
1033 Int J Parasitol. 2021;51:797–807. Available from:
1034 http://dx.doi.org/10.1016/j.ijpara.2021.04.006

1035 33. Podbilewicz B. Cell fusion. In: Kramer JM, Moerman DG, editors. WormBook: The online
1036 review of C elegans biology. The C. elegans Research Community; 2006 [cited 2024 Nov 7].
1037 Available from: http://www.wormbook.org/chapters/www_cellfusion/cellfusion.html#bib57

1038 34. Cantacessi C, Campbell BE, Young ND, Jex AR, Hall RS, Presidente PJA, et al.
1039 Differences in transcription between free-living and CO2-activated third-stage larvae of
1040 Haemonchus contortus. BMC Genomics. 2010;11:266. Available from:
1041 http://dx.doi.org/10.1186/1471-2164-11-266

1042 35. Cao J, Packer JS, Ramani V, Cusanovich DA, Huynh C, Daza R, et al. Comprehensive
1043 single-cell transcriptional profiling of a multicellular organism. Science. 2017;357:661–7.

1044 Available from: http://dx.doi.org/10.1126/science.aam8940

1045 36. Alfieri JM, Wang G, Jonika MM, Gill CA, Blackmon H, Athrey GN. A Primer for Single-
1046 Cell Sequencing in Non-Model Organisms. Genes. 2022;13. Available from:
1047 http://dx.doi.org/10.3390/genes13020380

1048 37. Evercode Fixation and WT v2 User Guides. Parse Biosciences; 2023. Available from:
1049 https://support.parsebiosciences.com/hc/en-us/articles/23915040729876-Evercode-Fixation-
1050 and-WT-v2-User-Guides

1051 38. Srivastava N, Nader GP de F, Williart A, Rollin R, Cuvelier D, Lomakin A, et al. Nuclear
1052 fragility, blaming the blebs. Curr Opin Cell Biol. 2021;70:100–8. Available from:
1053 https://pubmed.ncbi.nlm.nih.gov/33662810/

1054 39. Wakelin D. Acquired immunity to Trichuris muris in the albino laboratory mouse.
1055 Parasitology. 1967;57:515–24. Available from:
1056 http://dx.doi.org/10.1017/s0031182000072395

1057 40. White EC, Houlden A, Bancroft AJ, Hayes KS, Goldrick M, Grencis RK, et al.
1058 Manipulation of host and parasite microbiotas: Survival strategies during chronic nematode
1059 infection. Sci Adv. 2018;4:eaap7399. Available from:
1060 http://dx.doi.org/10.1126/sciadv.aap7399

1061 41. Duque-Correa MA, Karp NA, McCarthy C, Forman S, Goulding D, Sankaranarayanan G,
1062 et al. Exclusive dependence of IL-10Rα signalling on intestinal microbiota homeostasis and
1063 control of whipworm infection. PLoS Pathog. 2019;15:e1007265. Available from:
1064 http://dx.doi.org/10.1371/journal.ppat.1007265

1065 42. Hu P, Fabyanic E, Kwon DY, Tang S, Zhou Z, Wu H. Dissecting Cell-Type Composition
1066 and Activity-Dependent Transcriptional State in Mammalian Brains by Massively Parallel
1067 Single-Nucleus RNA-Seq. Mol Cell. 2017;68:1006–15.e7. Available from:
1068 http://dx.doi.org/10.1016/j.molcel.2017.11.017

1069 43. Habib N, Li Y, Heidenreich M, Swiech L, Avraham-Davidi I, Trombetta JJ, et al. Div-Seq:
1070 Single-nucleus RNA-Seq reveals dynamics of rare adult newborn neurons. Science.
1071 2016;353:925–8. Available from: http://dx.doi.org/10.1126/science.aad7038

1072 44. Habib N, Avraham-Davidi I, Basu A, Burks T, Shekhar K, Hofree M, et al. Massively
1073 parallel single-nucleus RNA-seq with DroNc-seq. Nat Methods. 2017;14:955–8. Available
1074 from: http://dx.doi.org/10.1038/nmeth.4407

1075 45. Lake BB, Ai R, Kaeser GE, Salathia NS, Yung YC, Liu R, et al. Neuronal subtypes and
1076 diversity revealed by single-nucleus RNA sequencing of the human brain. Science.
1077 2016;352:1586–90. Available from: http://dx.doi.org/10.1126/science.aaf1204

1078 46. Lacar B, Linker SB, Jaeger BN, Krishnaswami S, Barron J, Kelder M, et al. Nuclear
1079 RNA-seq of single neurons reveals molecular signatures of activation. Nat Commun.
1080 2016;7:11022. Available from: https://www.nature.com/articles/ncomms11022

1081 47. Nadelmann ER, Gorham JM, Reichart D, Delaughter DM, Wakimoto H, Lindberg EL, et
1082 al. Isolation of Nuclei from Mammalian Cells and Tissues for Single-Nucleus Molecular
1083 Profiling. Curr Protoc. 2021;1:e132. Available from: http://dx.doi.org/10.1002/cpz1.132

1084 48. Ewels P, Magnusson M, Lundin S, Käller M. MultiQC: summarize analysis results for
1085 multiple tools and samples in a single report. Bioinformatics. 2016;32:3047–8. Available
1086 from: http://dx.doi.org/10.1093/bioinformatics/btw354

49. Doyle SR, Tracey A, Laing R, Holroyd N, Bartley D, Bazant W, et al. Genomic and transcriptomic variation defines the chromosome-scale assembly of Haemonchus contortus, a model gastrointestinal worm. Commun Biol. 2020;3:656. Available from: http://dx.doi.org/10.1038/s42003-020-01377-3

50. Foth BJ, Tsai IJ, Reid AJ, Bancroft AJ, Nichol S, Tracey A, et al. Whipworm genome and dual-species transcriptome analyses provide molecular insights into an intimate host-parasite interaction. Nat Genet. 2014 [cited 2023 Nov 16];46:693–700. Available from: https://www.nature.com/articles/ng.3010

51. Hao Y, Stuart T, Kowalski MH, Choudhary S, Hoffman P, Hartman A, et al. Dictionary learning for integrative, multimodal and scalable single-cell analysis. Nat Biotechnol. 2024;42:293–304. Available from: https://www.ncbi.nlm.nih.gov/pmc/articles/PMC10928517/

52. Howe KL, Bolt BJ, Shafie M, Kersey P, Berriman M. WormBase ParaSite - a comprehensive resource for helminth genomics. Mol Biochem Parasitol. 2017;215:2–10. Available from: http://dx.doi.org/10.1016/j.molbiopara.2016.11.005

53. Kuleshov MV, Jones MR, Rouillard AD, Fernandez NF, Duan Q, Wang Z, et al. Enrichr: a comprehensive gene set enrichment analysis web server 2016 update. Nucleic Acids Res. 2016;44:W90–7. Available from: http://dx.doi.org/10.1093/nar/gkw377

54. Chen EY, Tan CM, Kou Y, Duan Q, Wang Z, Meirelles GV, et al. Enrichr: interactive and collaborative HTML5 gene list enrichment analysis tool. BMC Bioinformatics. 2013;14:128. Available from: http://dx.doi.org/10.1186/1471-2105-14-128

55. Kolberg L, Raudvere U, Kuzmin I, Adler P, Vilo J, Peterson H. g:Profiler-interoperable web service for functional enrichment analysis and gene identifier mapping (2023 update). Nucleic Acids Res. 2023;51:W207–12. Available from: http://dx.doi.org/10.1093/nar/gkad347

1127 # Supplementary Information

1128

1129 ## Optimisation of single-nuclei isolation and RNA sequencing of
1130 parasitic nematodes

1131

1132 Supplementary Figure 1. Fluorescence-Activated Cell Sorting (FACS) plots for sample-
1133 matched unstained negative controls. 2
1134 Supplementary Figure 2. Fluorescence-Activated Cell Sorting (FACS) gating strategy for
1135 nuclei.....3
1136 Supplementary Figure 3. Tapestation HS D5000 fragment trace analysis of Parse sub-
1137 libraries and final libraries. 4
1138

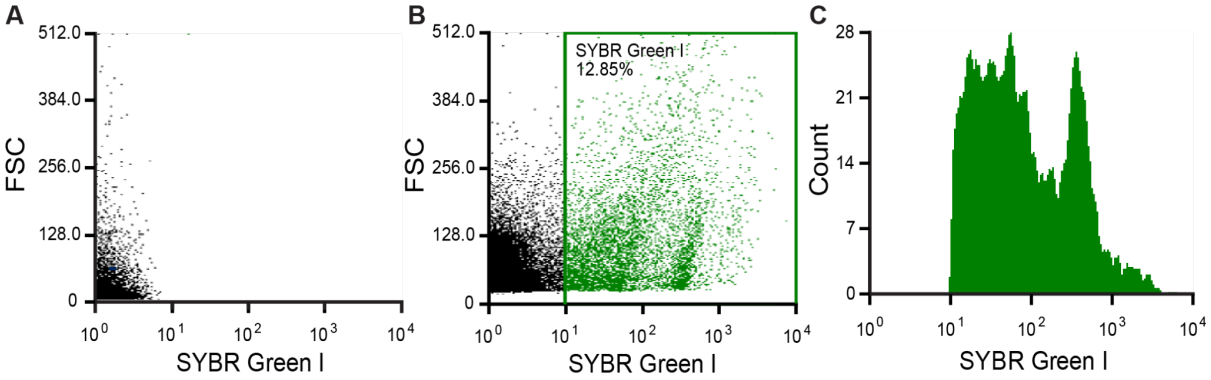

Supplementary Figure 1. Fluorescence-Activated Cell Sorting (FACS) gating strategy for nuclei.

Small debris from the nuclei suspensions was removed using FACS. A) A 50 µl aliquot of nuclei from each sample was used as a negative control for fluorescent staining detection levels. B) The remaining sample (~500 µl) was stained with 5 µl 1,000x SYBR Green I (ThermoFisher) and sorted on a positive fluorescent signal compared to the unstained control from the same nuclei suspension. The x-axis displays SYBR Green I fluorescence in log scale using the 488 nm laser and 507/19 filter. The y-axis is the forward scatter area (FSC-A) in linear scale. Cellular and cuticle debris is shown in black and is unstained with SYBR Green I.

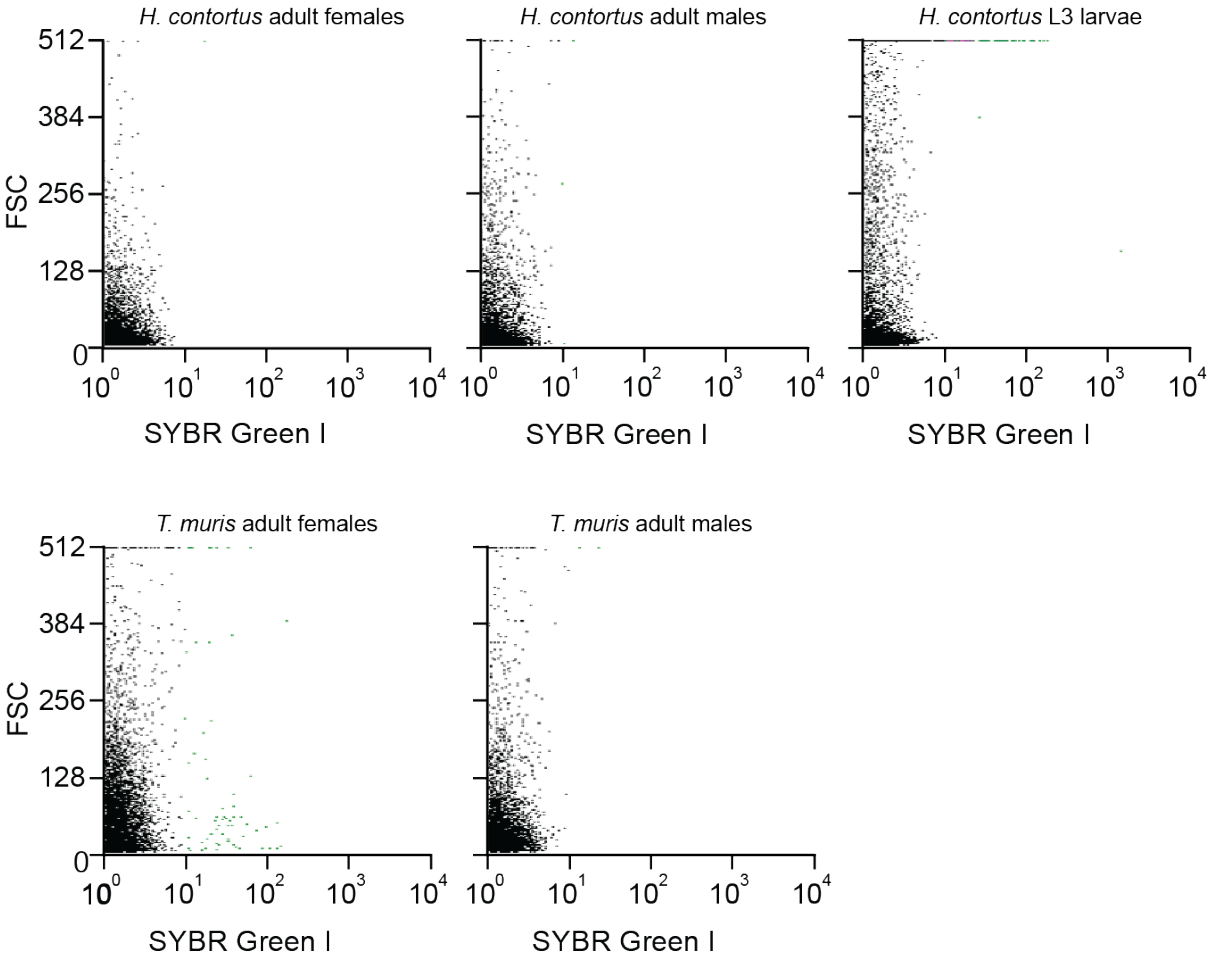

Supplementary Figure 2. Fluorescence-Activated Cell Sorting (FACS) plots for sample-matched unstained negative controls.

FACS plots of nuclei isolated from each species and life stage tested using the optimised nuclei isolation protocol. An aliquot of each nuclei isolation was used as an unstained negative control to determine gating for a positive SYBR Green I signal. The x-axis displays SYBR Green I fluorescence in log scale using the 488 nm laser and 507/19 filter. The y-axis is the forward scatter area (FSC-A) in linear scale.

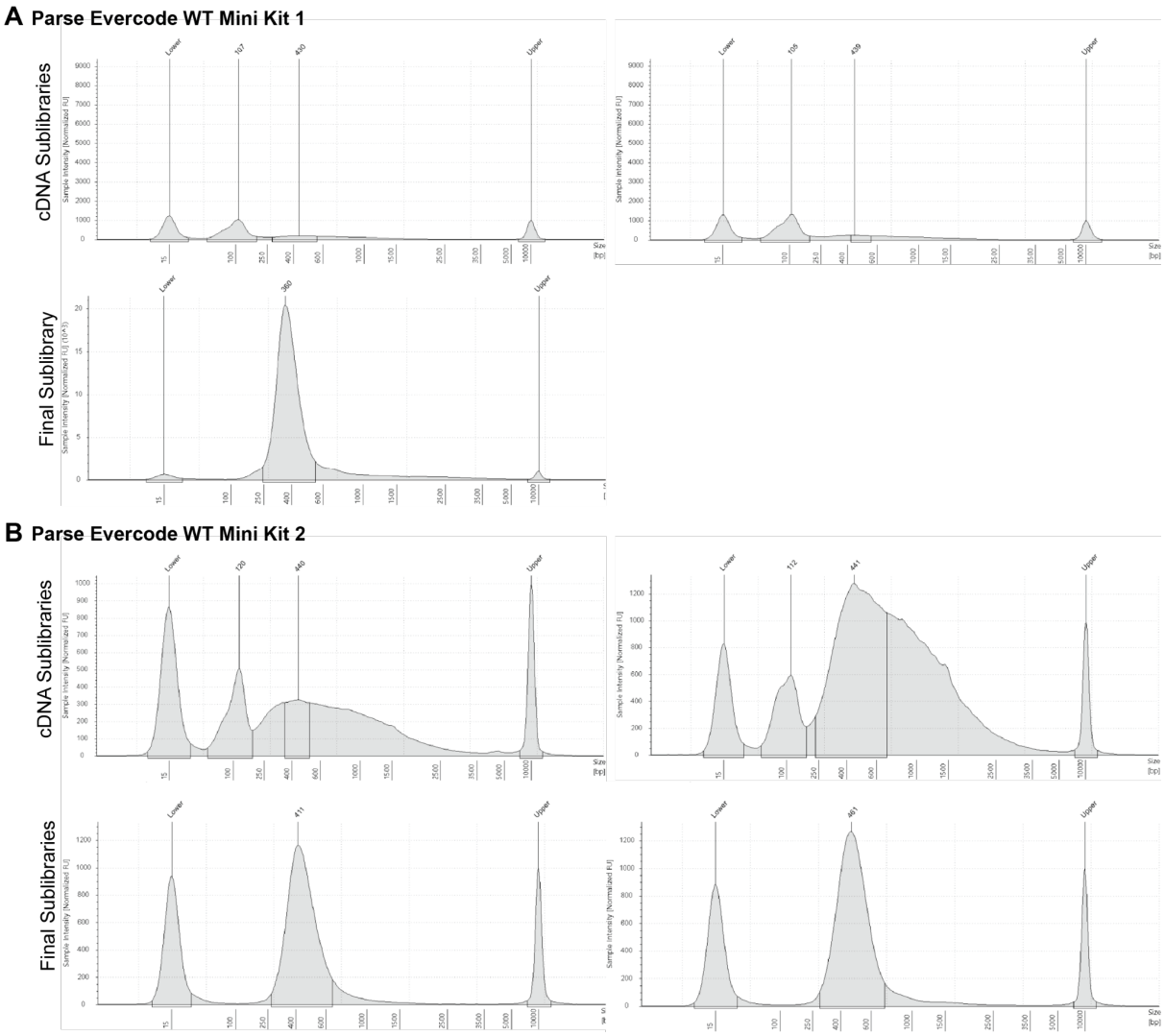

Supplementary Figure 3. Tapestation HS D5000 fragment trace analysis of Parse sub-libraries and final libraries.

A) Parse Evercode WT Mini Kit run 1 fragment traces of the two cDNA sub-libraries and the resulting final sub-library from the combined sublibraries. Qubit measurements for sublibraries 1 and 2 were 2.22 ng/µl and 2.12 ng/µl, respectively. The sublibraries were combined, and the remaining 60.76 ng cDNA was used for fragmentation, end repair, and A-tailing. The final library was quantified with Qubit as 18.6 ng/µl. B) Parse Evercode WT Mini Kit run 2 fragment traces of the two cDNA sub-libraries in a 1:2 dilution. Qubit measurements for sub-libraries 1 and 2 were 6 ng/µl and 12 ng/µl, respectively. 100 ng of each sub-library was used for fragmentation, end repair, and A-tailing. The two final indexed sub-libraries were assessed on the Tapestation in a 1:5 dilution. Qubit measurements for final libraries 1 and 2 were 6.34 ng/µl and 9.54 ng/µl, respectively.